ISSN 0024-4902, Lithology and Mineral Resources, 2015, Vol. 50, No. 1, pp. 50–79. © Pleiades Publishing, Inc., 2015.
Original Russian Text © B.A. Sakharov, V.A. Drits, 2015, published in Litologiya i Poleznye Iskopaemye, 2015, No. 1, pp. 55–86.

Technique for Determination of the Content of Smectite Layers in the Dispersed Dioctahedral K-Bearing Micaceous Minerals

B. A. Sakharov and V. A. Drits

Geological Institute, Russian Academy of Sciences, Pyzhevskii per. 7, Moscow, 119017 Russia
e-mail: sakharovba@gmail.com

Received March 26, 2014

Abstract—A technique was developed to determine the low contents of smectite layers in the dispersed dioctahedral K-bearing micaceous minerals of the illite–glauconite composition. To implement this technique, diffraction patterns were calculated for two-component mixed-layer mica–smectite structures, in which the content of smectite layers increased with a step of 2% from 2 to 20% at a short-range order factor $R = 0$ and from 2 to 14% at $R = 1$. On the basis of Mering's principles (1949) and Q-rules (Moore and Reynolds, 1989), the half-width $\beta\cos\theta$ of each basal refection and its distance Q to the nearest reflection corresponding to the periodical structure made up of 9.98 Å micaceous layers were calculated for mixed-layer structures with the given content of smectite layers W_{Sm}. The Q dependence on $\beta\cos\theta$ for the series of basal reflections observed in the calculated diffraction pattern was approximated by a straight line corresponding to the linear regression equation. Equations relating slope angles of straight line (α) and concentrations of smectite layers (W_{Sm}) were deduced for the analyzed mixed-layer structures with the short-range order factors $R = 0$ and $R = 1$, respectively. To determine the contents of smectite layers in natural micaceous varieties, the basal reflections observed in experimental patterns from the oriented ethylene glycol-saturated samples were subjected to the following procedures: (1) determination of the half-width $(\beta\cos\theta)_e$ of each $00l$ reflection of the analyzed sample and plotting Q dependence on $(\beta\cos\theta)_e$ for the observed series of basal reflections, with its further approximation by the linear regression equation and the corresponding straight line; (2) calculation of the slope angle of this straight line α and determination of the content of smectite layers in the sample structure using the equation relating α and W_{Sm}. Application of the described procedure showed that the content of smectite layers in the studied samples varied from 5.2 to 12.6%. The content of smectite layers was determined accurate to a few tenths of a percent. Since the half-width of reflection 003 does not depend on the content of smectite layers, its value was used to determine the thickness and number of layers in the averaged CSD of the studied sample. XRD patterns calculated for mixed-layer structures with experimentally determined W_{Sm}, W_{Mc}, R, T, and N parameters are in a good agreement with experimental patterns of the studied samples.

DOI: 10.1134/S0024490215010058

INTRODUCTION

Finely dispersed dioctahedral K-bearing micaceous minerals are widespread in diverse geological settings of the Earth's crust (Środoń, 1999; Moore and Reynolds, 1989, 1997; Drits and Kossovskaya, 1990, 1991; Drits et al., 1983). Idealized structure of these minerals is made up of 2 : 1 layers linked by interlayer K cations. Each 2 : 1 layer is composed of an octahedral sheet sandwiched between tetrahedral sheets. In the dioctahedral 2 : 1 layers, two of three symmetrically independent octahedra are occupied by cations. Succession of 2 : 1 layers forms one-layer monoclinic structure corresponding to 1M polytype. In natural samples, such periodicity is often disturbed due to stacking faults caused by the relative rotation of adjacent layers at ±120°or $n60°$ ($n = 0, 1, 2, ..., 5$). Idealized structural formula of the considered mineral group can be represented as follows:

$$K_{x+y}(Si_{4-x}Al_x)(R^{3+}_{2-y}R^{2+}_y)O_{10}(OH)_2,$$

where R^{3+} and R^{2+} correspond to the trivalent (Al, Fe^{3+}) and divalent (Mg, Fe^{2+}) octahedral cations, respectively.

Depending on the cationic composition of octahedral and tetrahedral sheets of 2 : 1 layers, the following main mineral varieties are distinguished: illites ($x > 0.2$; $R^{3+} > R^{2+}$, $Al > Fe^{3+}$), glauconites ($x > 0.2$; $R^{3+} > R^{2+}$, $Fe^{3+} > Al$), aluminoceladonites ($R^{3+} \approx R^{2+}$, $Al > Fe^{3+}$, $x < 0.2$), and celadonites ($R^{3+} \approx R^{2+}$, $Fe^{3+} > Al$, $x < 0.2$). All low-temperature (i.e., formed at T < 150°C) dioctahedral K-bearing micaceous minerals are characterized by two features. First, the interlayer K cations occupy most, but not all available, interlayer sites. Therefore, the sum of K cations in the micaceous interlayers ($x + y$) varies for different samples between 0.65 and 0.85 (Środoń et al., 1986; Sakharov et al., 1990, 1999) as calculated per $O_{10}(OH)_2$. Second, the interlayer spaces of the considered mineral group, as the predominant micaceous layers, contain a minor amount of expandable smectite interlayers. In other words, the finely dispersed dioctahedral micaceous

minerals usually have a mixed-layer structure, in which up to 20% of smectite interlayers are distributed between micaceous layers with variable order-disorder degree (Reynolds, 1980, 1988; Drits and Sakharov, 1976; Drits and Tchoubar, 1990).

Determination of the content and alternation order of micaceous and smectite interlayers in the mixed-layer illite–smectite and glauconite–smectite structures is discussed in (Reynolds and Hower, 1970; Reynolds, 1985; Drits and Sakharov, 1976; Drits et al., 1983, 2010; Drits and Tchoubar, 1990; McCarty et al., 2009; Środoń et al., 1980, 1981, 1984; Sakharov and Lanson, 2013). The most efficient approach to the structural study of sample is obtaining the best fit between the calculated and experimental XRD patterns containing basal reflections. It is believed that the structural parameters, at which the best fit is attained, adequately describe the sample structure (Sakharov et al., 1999; Drits et al., 1997b, Lanson et al., 2009; Drits et al., 2005). Such an approach is sufficiently time-consuming and requires the application of special softwares. Therefore, in practice the structural characteristics of mixed-layer minerals are usually determined by another method. To implement this method, several researchers (Drits and Sakharov, 1976; Reynolds, 1980, 1988; Drits et al., 1983; Środoń, 1980, 1981, 1984; Watanabe, 1981) carried out systematic calculations of XRD patterns for the dioctahedral mixed-layer illite–smectites and glauconite–smectites, which differ in the content and distribution pattern of different layers.

These data were used to determine the diffraction criteria, which allow the identification of a certain mixed-layer phase without preliminary calculations. Moreover, a series of graphical methods was proposed to establish the types of layers, their concentrations, and distribution. These methods are based on the analysis of positions of basal reflections recorded on XRD pattern from the oriented ethylene glycol-saturated specimens. It is obvious that the lower the content of smectite layers in the micaceous sample structure, the weaker their influence on the position of basal reflections. At sufficiently low contents of smectite layers, the position of basal reflections depends on the thickness of the coherent scattering domains (CSDs) and instrumental factors rather than on concentrations of expandable interlayers. Under these conditions, the graphical methods reported in literature seem to be low efficient, because they do not provide accurate determination of small amounts of smectite layers in the structure of mixed-layer minerals.

Moore and Reynolds (1989) based on Mering's principals (Mering, 1949) proposed another way to determine the low contents of layers of one type in a matrix of another layer type. According to one of these principles, broadening of the basal reflection of mixed-layer structure with random distribution of *A* and *B* layers depends on its distance to the nearest basal reflection, which corresponds to the periodical structure consisting of either layers A or layers B. This offers an opportunity to determine the minor contents of a component by analyzing the broadening of basal reflections observed in the XRD pattern of a two-component mixed-layer structure.

The main advantage of the proposed approach is as follows: it does not require the determination of exact position of basal reflections from the analyzed mixed-layer sample. Unfortunately, Moore and Reynolds (1997) did not provide a detailed description of physical principles underlying the "*Q* rule," which was recommended to use for estimating the degree of broadening of basal reflections corresponding to a certain mixed-layer phase. For this reason, as far as we know, *Q*-rule has not yet been applied for the analysis of natural mixed-layer phases.

The aim of this work was to consider in detail the methodological aspects of this approach, its opportunities and limitations with respect to the highly dispersed dioctahedral varieties of K-bearing micaceous minerals (illites and glauconites), which contain small amounts of expandable smectite layers and have relatively thin CSDs. This problem was solved using software allowing the simulation of diffraction patterns from structural models of the considered group of micaceous minerals with small amounts of smectite layers. High efficiency of the application of this program was exemplified by the study of diverse natural mixed-layer minerals (Drits et al., 2011; Drits et al., 1997b, 2002a, 2005; Sakharov et al., 1999; Lanson et al., 2009; Lindgreen et al., 2002, 2008; McCarty et al., 2008, 2009).

OBJECTS AND METHODS

We studied the globular dioctahedral micaceous glauconite–illite varieties collected from the Upper Proterozoic successions of North Siberia and described in detail by Ivanovskaya et al. (2012). Sample names in the present paper are as in the above work. In addition, we studied glauconite sample 37/71 from the Lower Ordovician of Latvia (collection of T.A. Ivanovskaya) and the hydrothermal illite sample RM30, which represents the standard accepted by the Clay Mineralogical Society (CMS) of the United States. The structural–mineralogical characteristics of the latter sample is reported in (Drits et al., 2010). Oriented specimens prepared by the method of particle precipitation from suspension less than 0.001 mm in size were studied using a Bruker D-8 diffractometer. Diffraction patterns were recorded using Cu$K\alpha$ radiation on points within 2θ angle range from 2.00° to 80.00° with a step of 0.05° 2θ, exposure 80 s, acceleration voltage 40 kV, and beam current 40 mA. The goniometer radius was 250 mm, divergence and antiscatter slits established immediately after the X-ray tube were 0.5°, and the width of the receiving slit in front of the scintillation detector was 0.1 mm.

METHODOLOGY

Calculation of XRD Patterns

The XRD patterns containing basal reflections were calculated for the models of mixed-layer mica–smectite structures using a software proposed by B.A. Sakharov and A.S. Naumov based on algorithms described in monographs by Drits and Sakharov (1976) and Drits and Tchoubar (1990), as well as in the review by Sakharov and Lanson (2013). The effect of instrumental parameters, such as vertical and horizontal divergence of incident and diffracted X-ray beams, diameter of goniometer, and size and thickness of samples, were taken into account according to recommendations of Reynolds (1986) and Drits et al. (1983).

A mixed-layer structure with alternation of micaceous (Mc) and smectite (Sm) layers will be designated as Mc–Sm. Interlayer sites of such structures are filled, respectively, by K cations for the micaceous interlayers and by ethylene glycol molecules and exchange cations for the smectite interlayers. For micaceous and smectite layers of the mixed-layer Mc–Sm phase, *z*-coordinates and site occupancy by the corresponding atoms were determined according to (Moore and Reynolds, 1997). The K content in the interlayers accounted for 0.75 atoms per formula unit (f.u.), i.e. per anionic framework $O_{10}(OH)_2$ of 2 : 1 layer. K cations were placed at centers of micaceous interlayers. The thickness of micaceous layer (2 : 1 layer plus interlayer) and smectite layer was 9.98 Å and 16.85 Å, respectively.

The CSD thickness, which is determined by the number of strictly parallel layers of different nature, varied according to the lognormal distribution–its average and maximal values were variable parameters (Drits et al., 1997a).

Statistical Description of Mixed-Layer Structures

In order to calculate the diffraction effects from the mixed-layer structure, it is necessary to determine the number of alternating types of layers, their structure and distribution in a crystallite, as well as sizes of the CSD (Drits and Sakharov, 1976; Sakharov and Lanson, 2013). First of all, to determine the order of alternating layers, it is necessary to know the relative contents of layers of each type (W_i). Another important parameter is the so-called short-range order factor (R), which is equal to the number of preceding layers that defines the probability of the appearance of a specified layer. If layers of different types have random distribution, the appearance of any layer does not depend on the nature of preceding layer and $R = 0$; if the preceding layer affects the next layer, $R = 1$; and so on. However, parameter R does not define the nature of this influence, which is characterized by conditional probability parameters. For the mixed-layer structure in which layers A and B with relative contents W_A and W_B are interstratified at $R = 1$, the sequence of layer types in the crystal or CSD may be described using four conditional probabilities (P_{AA}, P_{AB}, P_{BA}, P_{BB}). Probability of the occurrence of layer pairs of *AB* or *BB* types equals $W_A P_{AB}$ and $W_B P_{BB}$, respectively. Probability of the occurrence of any layer subsequence can be calculated by similar way. For instance, probability of the occurrence of *AABAB* sequence is $W_A P_{AA} P_{AB} P_{BA} P_{AB}$. Six probability parameters interdepend by the following relationships:

$$W_A + W_B = 1; \quad P_{AA} + P_{AB} = P_{BA} + P_{BB} = 1;$$

$$W_A P_{AB} = W_B P_{BA}.$$

Therefore, only two independent parameters should be known to describe a two-component structure with $R = 1$. If $W_A > W_B$, such parameters can be W_B and P_{BB}, because $W_A = 1 - W_B$, $P_{BA} = 1 - P_{BB}$, $P_{AB} = W_B(1 - P_{BB})/(1 - W_B)$, and $P_{AA} = [1 - W_B(2 - P_{BB})]/(1 - W_B)$.

Note some characteristic relationships between probability parameters. If $P_{BB} = 0$ and $W_A > W_B$, the studied structure is characterized by maximum possible degree of order in the alternation of layers *A* and *B* at $R = 1$. In a structure with $P_{AA} = W_A$ and $P_{BB} = W_B$, $R = 0$ and layers of different types show completely random distribution. For mixed-layer structures with short-range order factor $R = 2$ or 3, the position of a definite layer depends on two or three preceding layers. For this reason, coefficients P_{ikl} (i, k, $l = A$, B) or P_{iklm} (i, k, l, $m = A$, B) are introduced to describe the alternation of layers in the two-component mixed-layer structure with $R = 2$ or 3, respectively. Under these conditions, coefficient P_{AAB} determines the probability that layer *B* will follow the doublet *AA* in the chosen direction. Similarly, if $R = 3$, coefficient P_{ABAB} determines the probability that layer *B* will follow the triplet *ABA*. Among all diversity of mixed-layer structures with $R = 2$, we distinguish only structures with $W_A \geq 0.67$ and maximum possible degree of ordering in the alternation of layers of different types. For such structures, both P_{BB} and P_{BAB} should have zero values. If two layers B in structures with $R = 1$ and maximum possible degree of order do not occur together ($P_{BB} = 0$), but they can be separated by one layer *A* (i.e., *BAB* combination is allowed), two B layers in the model with $R = 2$ should be separated by at least two layers *A*. Under these conditions, the layer succession in crystals with $R = 2$, $W_A \geq 2/3$, and $P_{BAB} = 0$ may be described knowing only one independent parameter (W_B). Similarly, the maximum possible degree of ordering in the alternation of layers of different types in two-component mixed-layer structures with $R = 3$ and $W_A \geq 0.75$ is attained if $P_{BB} = P_{BAB} = P_{BAAB} = 0$. Again, as for structure with $R = 1$ and $R = 2$, the alternation of layers with the maximum possible degree of order at $R = 3$ and $W_A \geq 0.75$ may be described by only one independent parameter, W_B.

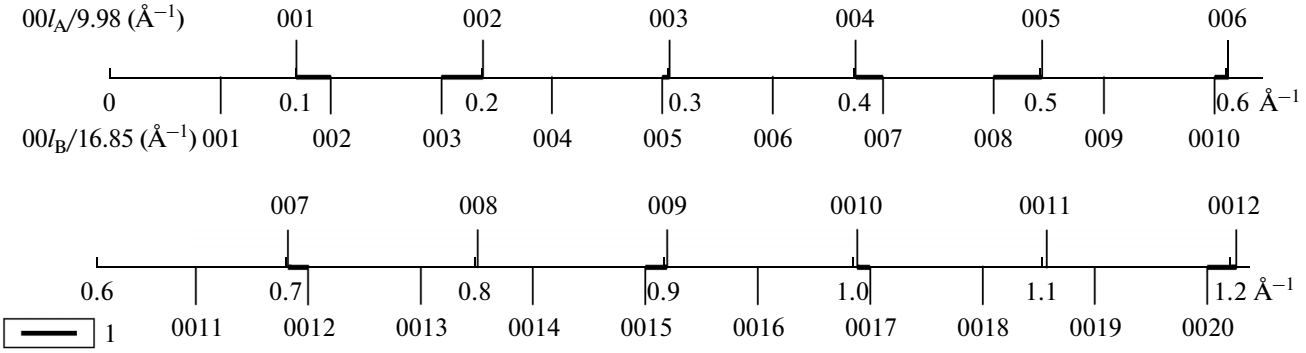

Fig. 1. Graphic image of nodes of reciprocal lattice along the c^* axis corresponding to reflections 00l for periodical structures with the layer thickness of 9.98 and 16.85 Å, respectively. (1) Areas in which reflections of a mixed-layer phase may be located.

Mering's Principles

Mering (1949) formulated principles allowing the simplest way to describe the formation of XRD pattern from two-component mixed-layer structures with a random alternation of A and B layers. According to the first principle, each node of reciprocal lattice corresponding to the mixed-layer structure may be situated along c^* axis of this lattice between the closest nodes corresponding to the periodical structures, which consist of either A or B layers. For instance, if periods along normal to the layers of the periodic structures are equal to $d(001)_A$ and $d(001)_B$, their periods along c^* axis in the reciprocal lattice will equal $r_A^* = 1/d(001)_A$ and $r_B^* = 1/d(001)_B$, respectively. Thus, the nodes of reciprocal lattices of the periodic structures are situated along the c^* axis in succession $l_A r_A^*$ and $l_B r_B^*$, where l_A and l_B are integers corresponding to the indices of corresponding nodes. In Fig. 1 showing the mutual positions of nodes $l_A r_A^*$ and $l_B r_B^*$ ($r_A^* = 0.1002$ Å^{-1} and $r_B^* = 0.0593$ Å^{-1} correspond to $d(001)_A = 9.98$ Å and $d(001)_B = 16.85$ Å), we distinguish areas between the closest nodes $l_A r_A^*$ and $l_B r_B^*$, which should contain nodes of the reciprocal lattice of the mixed-layer phase. Each node of the reciprocal lattice corresponds to the basal reflection in the XRD pattern of sample having periodic or mixed-layer structure. Thus, according to Mering's first principle, each basal reflection recorded from the random mixed-layer phase must be located between two reflections corresponding to periodical structures consisting of layers A and B. The position of 00l reflection corresponding to the mixed-layer phase in a first approximation depends on the concentrations of layers A and B (W_A and W_B) according to the following equation:

$$1/d(00l)_{obs} = W_A/d(00l)_A + W_B/d(00l)_B, \qquad (1)$$

where $d(00l)_A$ and $d(00l)_B$ are spacings of reflections of periodic structures consisting of layers A and B, which sandwich a reflection of the mixed layer phase with spacing $d(00l)_{obs}$ at the given W_A and W_B values. It follows from Eq. (1) that the lower the content of layers B (W_B), the closer the basal reflections of the mixed-layer phase are to the reflections of periodical structure consisting of layers A. At a very low content of layers B, the XRD pattern of the corresponding mixed-layer structure will only show reflections located near the reflections of periodical phase consisting of layers A. Therefore, such reflections are identified using the same indices 00l that are used for reflections of the periodical structure. The above-mentioned facts should be taken into account during the consideration of diffraction patterns of random two-component mixed-layer structures with a low content of one of the components.

According to Mering's second principle, the longer the distance between the adjacent basal reflections corresponding to the periodical structures, the broader located between them the basal reflection corresponding to the mixed-layer phase. All above-mentioned features following from Mering's principles are clearly seen in the diffraction pattern calculated for the ethylene glycol-saturated random mixed-layer mica–smectite phase containing 80% micaceous interlayers (Fig. 2a). Vertical lines mark the positions of basal reflections corresponding to the periodical structures of 9.98 Å mica and 16.85 Å smectite, with basal reflections of the mixed-layer phase between them. These reflections become broader with increasing distance between the limiting reflections of periodical structures (Fig. 2a).

Drits and Sakharov (1976) and Drits et al. (1997) expanded the possibilities of Mering's principles and demonstrated their applicability to two-component mixed-layer structures, in which layers A and B are alternated with maximum possible degree of order (MPDO) at a short-range order factor $R = 1$, 2, or 3. As already mentioned, if at $R = 1$ and $W_A > W_B$, layers of different types are alternated with MPDO, then a mixed-layer structure is devoid of layer pairs BB, i.e.,

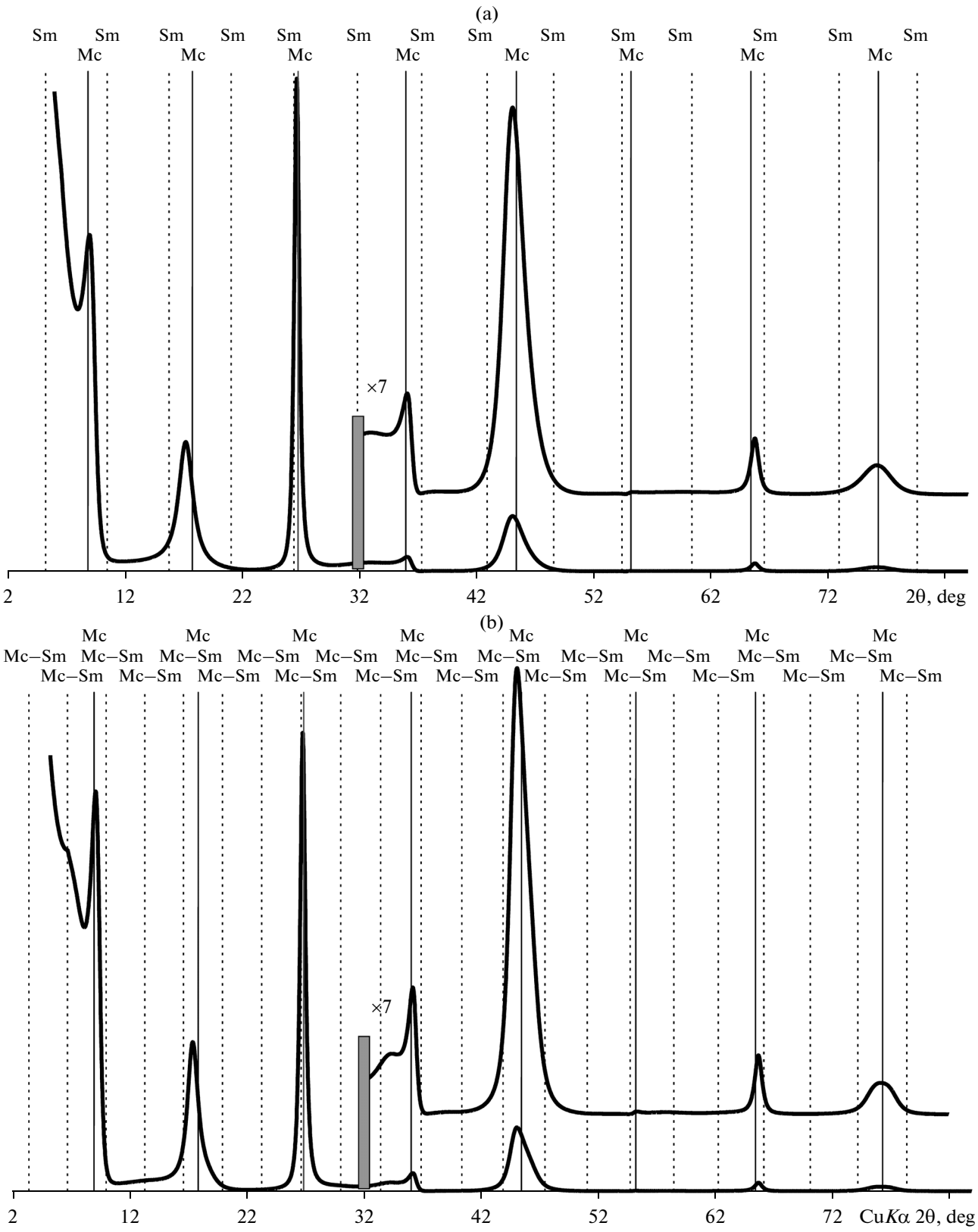

Fig. 2. Diffraction patterns calculated for the ethylene glycol-saturated disordered mixed-layer mica–smectite phase containing 80 and 86% of 9.98 Å micaceous, and, respectively, 20 and 14% of 16.85 Å smectite layers alternating with short-range order factor: (a) $R = 0$; (b) $R = 1$. Solid and dashed vertical lines correspond to the positions of basal reflections 00*l* for periodical structures of: (a) mica (Mc) and smectite (Sm); (b) mica (Mc) and mica–smectite layer pairs (Mc–Sm).

$P_{BB} = 0$. Such structure can be described as the result of completely disordered alternation of layers A and layer pairs AB in accordance with Mering's principles. For instance, if structures with $R = 1$ is represented by alternation of 9.98 Å illite and 16.85 Å smectite layers in proportions 86 : 14, it may be considered as a structure with the random alternation (83.7 : 16.3) of 9.98 Å illite (A) and 26.83 Å rectorite (AB) layers. According to Mering's principles, the position and degree of broadening of basal reflections of such mixed-layer structure will depend on the mutual position of reflections corresponding to the periodical illite and rectorite structures (Fig. 2b).

Detailed description of the behavior of reflections, which, according to Mering's principles, should be observed in the XRD pattern of two-component mixed-layer structures, in which layers of different types are alternated with the maximum possible degree of order at $R = 2$ and 3, was given by Drits and Sakharov (1976) and in more detail by Drits et al. (1997).

The Q-rule

Moore and Reynolds (1989) proposed a method to obtain the quantitative information on the mixed-layer structure with a low concentration of one of the alternating layers. However, this method was sufficiently formally described. These authors considered the model of mixed-layer structure, in which a small (a few percents) amount of 10 Å biotite layers is alternated with 14.2 Å chlorite layers. The 10/14.2 ratio was multiplied by integers l corresponding to the orders of chlorite basal reflections. Then, the deviation of this value from the closest integer was found for each l 10/14.2 value and the result of this operation yielded the Q value. These values at different l predicted the degree of broadening of basal reflections of the mixed-layer chlorite–biotite phase: the higher the Q value, the more the degree of broadening of the corresponding reflection. To test this hypothesis, the diffraction pattern was calculated for the random mixed-layer biotite–chlorite structure containing 10% of biotite layers. It was found that Q values are related by practically linear dependence with half-widths of basal reflections. The latter values were multiplied by cosθ to exclude the effect of angular broadening of reflections from CSDs size. Moore and Reynolds concluded that the slope of straight lines relating Q with half-width of reflections at their half-thickness and calculated for different concentrations of biotite in mixed-layer structures may be used to determine the amount of biotite layers in these structures. However, such calculations are not presented in (Moore and Reynolds, 1998). As far as we know, correlation between Q values and half-widths of basal reflections has not been applied so far to study the natural mixed-layer structures with a minor amount of one of the components. This is possibly related to the fact that the method proposed by the above authors to determine Q does not explain its direct relation with Mering's principles, although this relation is undoubtedly present in a hidden form.

To provide insight into relationships between Q values and Mering's principles, let us again consider Fig. 1 demonstrating the mutual positions of reciprocal lattice nodes with indices $00l_A$ and $00l_B$ corresponding to the periodical structures consisting of layers A and B, respectively. It is well seen that each reflection $00l_A$ of phase A with the given l_A value is sandwiched between two reflections $00l_B$ and $(00l_B + 1)$ of phase B, and the distance to each of them is different. Exceptions are reflections 005_A and 008_A of phase A. The latter reflection is situated exactly in the middle between reflections 0013_B and 0014_B, while the former reflection is almost in the middle between reflections 008_B and 009_B of phase B. This denotes that the distance between reflections 008_A and 0013_B (or 0014_B) of phase B is the maximum possible and equals 0.5 in fractions of period r_B^* or $0.5\ r_B^*$ (Å^{-1}). Reflection 005_A has a similar position with respect to reflections 008_B and 009_B (Fig. 1). Each of the remaining reflections of phase A is always coupled with the reflection of phase B located at a distance of less than 0.50 (in fractions of period r_B^*) (Fig. 1).

Let us consider the relationship $l_A r_A^* / r_B^* = l'_B$, where l'_B shows how many times the distance between coordinate origin and node $00l_A$ of phase A (with the given l_A value) is greater than the period r_B^*. If l'_B equals integer l_B, the position of nodes $l_A r_A^*$ and $l_B r_B^*$ will coincide, while the half-width of basal reflection $00l$ with $l' = l_B$, observed in the XRD pattern of the mixed layer phase with a minor content of layers B will be equal to the half-width of reflection $00l$ of phase A. If l'_B will be $n + 0.500$, the distance between reflection $00l_A$ of phase A and closest reflections $00l_B$ ($l_B = n$) and $00(l_B + 1)$ of phase B is maximum possible. Hence, the corresponding node of the mixed-layer phase will have the maximum possible broadening. In order to determine the closest distance for the remaining pairs of nodes $00l_A$ and $00l_B$ in ratio $l_A r_A^* / r_B^*$ the valuel l_A should successively be increased. As seen from Fig. 1, the r_A^* / r_B^* ratio at $l_A = 1$ will be much higher than 1.5. Hence, reflection 002 of phase B will be the closest to reflection 001 of phase A, while Q value will be $\left|(2r_B^* - r_A^*)/r_B^*\right| = |2 - r_A^*/r_B^*|$. Conversely, the $2r_A^*/r_B^*$ ratio will be <3.5 and $Q = |(2r_A^* - 3r_B^*)/r_B^*| = |2r_A^*/r_B^* - 3|$ for reflection 002 of phase A. In other

Table 1. Calculated Q values for the mixed-layer structures with alternation of smectite (Sm) and micaceous (Mc) layers 16.85 and 9.98 Å thicknesses or layer pairs (Mc–Sm) and micaceous layers (Mc) 26.83 and 9.98 Å thicknesses

l	$l \times 16.85/9.98$	$l \times 26.83/9.98$	Q
1	1.688	2.688	0.312
2	3.377	5.377	0.377
3	5.065	8.065	0.065
4	6.754	10.754	0.246
5	8.442	13.442	0.442
6	10.130	16.130	0.130
7	11.819	18.819	0.181
8	13.507	21.507	0.493
9	15.195	24.195	0.195
10	16.884	26.884	0.116
11	18.572	29.572	0.428
12	20.261	32.261	0.261

l—order of basal reflection.

words, the deviation of l'_B in $l_A r^*_A / r^*_B$ ratios from the closest integer often corresponds to Q value.

Let us calculate Q values for mixed-layer structures under consideration, in which the predominant micaceous layers are alternated with smectite layers either randomly ($R = 0$) or with maximum possible degree of order at $R = 1$. In the first case, layers of 9.98 Å and 16.85 Å are alternated; in the second case, pairs Mc–Sm with a thickness of 26.83 Å and mica layers Mc with a thickness of 9.98 Å. Under these conditions, the 26.83/9.98 and 16.85/9.98 ratios should be multiplied by integers l_A corresponding to orders of mica basal reflections. As seen from Table 1, different Q values should predict the broadening for different orders of basal reflections of the mixed-layer phase regardless of definite contents of expandable layers. In the considered mixed-layer structures, the largest broadening is inferred for reflections 008, 005, and 0011, whereas reflections having indices 003, 0010, and 006 should be much narrower (Fig. 1). Reflection 003 with the least Q value should have the least broadening and minimum sensitivity to the content of expandable component. It should be emphasized that indices 00l in this example correspond to reflections of the mixed-layer phase, because 00l sequence of reflections at the minor content of expandable layers is similar in the diffraction patterns of both mixed-layer and periodic mica structures. Note at last that mixed-layer structures with $R = 0$ and $R = 1$ have similar Q values, because 26.83/9.98 and 16.85/9.98 differ by unity (Table 1).

Choice of Mc–Sm Models Depending on the Content of Smectite Layers at Different Factors R

As already mentioned, the Mc–Sm structures at the same content of smectite layers differ in the order of their distribution among the micaceous layers, which are characterized by the short-range order factor R. It is obvious that the different order of layer alternation at each given content of smectite layers will distort the diffraction pattern of the corresponding structure. To visualize the effect of different degrees of order on the alternation of different layers in Mc–Sm structures, we analyzed diffraction patterns of Mc–Sm structures, in which the relative content of smectite layer (W_{Sm}) subsequently changed with a step of 0.02 from 0 to 0.20, and the short-range order factor R at each W_{Sm} equals 0, 1, 2, or 3. Among all diversity of structures, only structures with the maximum possible degree of order were analyzed for each R value. This denotes that at $W_{Mc} > W_{Sm}$ and factors R equal 1, 2, and 3, the closest pairs of smectite layers are separated by at least one, two, or three micaceous layers, respectively. Smectite interlayers in the analyzed structures contain two layers of ethylene glycol molecules, and the thickness of smectite layer (2 : 1 layer + interlayer) was 16.85 Å.

The task was to distinguish structures, whose diffraction patterns unambiguously indicate the alternation of layers of different types with $R \geq 1$. Figures 3a–3c demonstrate four diffraction patterns corresponding to the Mc–Sm structures with different $W_{Mc} : W_{Sm}$ values. These structures have similar contents of smectite layers and the maximum possible order in the distribution of layers of different types at $R = 0$, 1, 2, and 3. At first, we exclude Mc–Sm structures with $R = 0$ and $W_{Sm} < 0.20$, because their diffraction patterns contain only basal reflections, the number and position of which is close to 00l reflections of mica (Figs. 3a–3c). Comparison of diffraction patterns calculated for Mc–Sm structures, which have similar $W_{Mc} : W_{Sm}$ at $R = 1$ and $R = 0$, demonstrates that they insignificantly differ in both intensity and position of basal reflections at $W_{Sm} \leq 0.14$. The weak low-angle reflection with $d =$ 13.04 Å observed in the calculated diffraction pattern and corresponding to the Mc–Sm structure with $W_{Mc} : W_{Sm} = 0.86 : 0.14$ can hardly appear under experimental conditions. At $W_{Sm} > 0.14$ and $R = 1$, an additional reflection with d = 12.91–13.0 Å was recorded in the low-angle region (Figs. 3b, 3c). The diffraction patterns of mixed-layer structures, in which the micaceous and smectite layers are alter-

Fig. 3. Diffraction patterns calculated for the mixed-layer mica–smectite structures (Mc–Sm) with alternating 9.98 Å micaceous (Mc) and 16.85 Å smectite (Sm) layers and maximum possible degree of order with $R = 0$, 1, 2, and 3 at $W_{Mc} : W_{Sm}$: (a) 0.90 : 0.10 and 0.88 : 0.12; (b) 0.86 : 0.14 and 0.84 : 0.16; (c) 0.82 : 0.18 and 0.80 : 0.20.

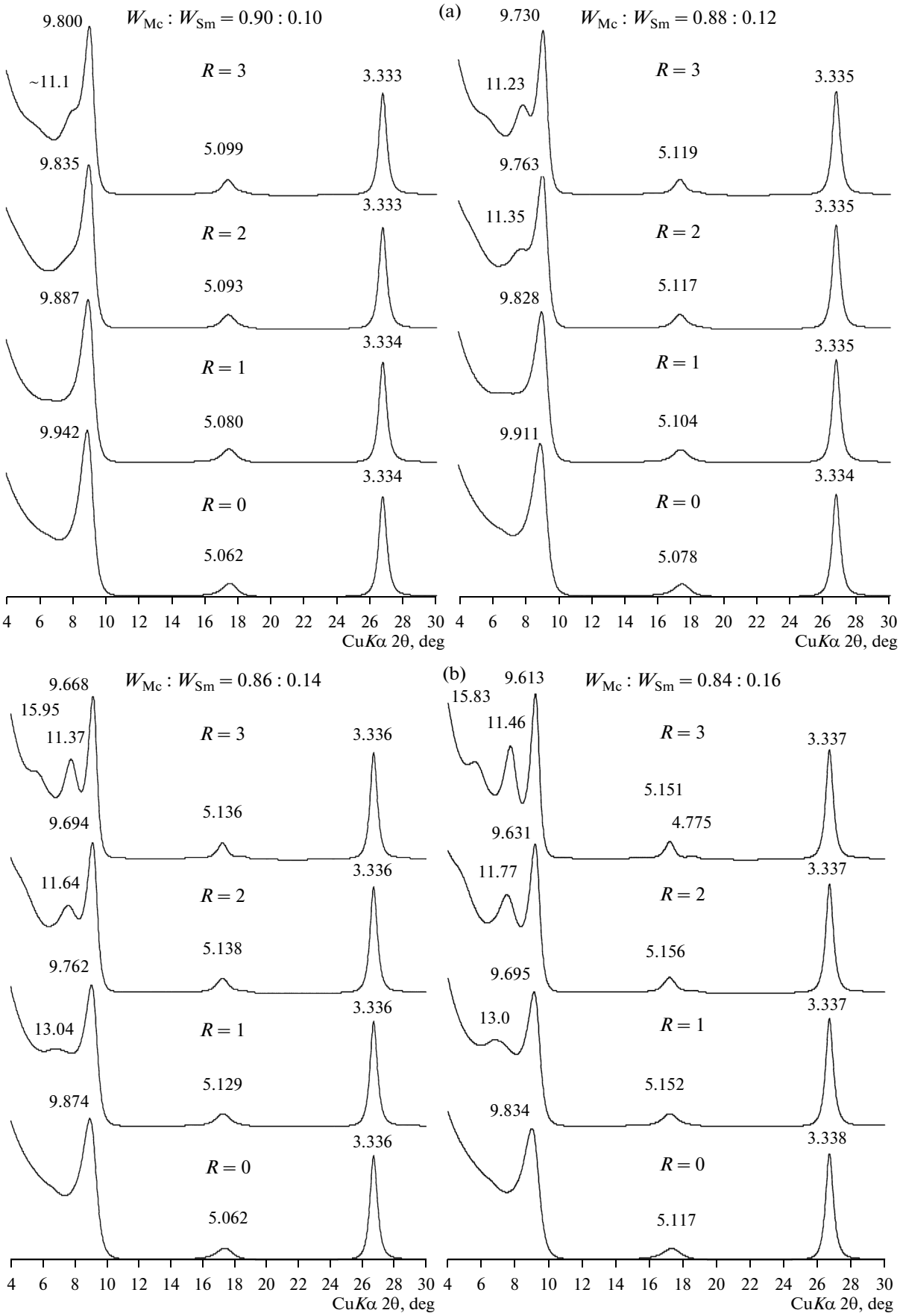
(a)
$W_{Mc} : W_{Sm} = 0.90 : 0.10$
9.800
~11.1
3.333
5.099
$R = 3$
9.835
3.333
5.093
$R = 2$
9.887
3.334
5.080
$R = 1$
9.942
3.334
5.062
$R = 0$
$W_{Mc} : W_{Sm} = 0.88 : 0.12$
9.730
11.23
3.335
5.119
$R = 3$
9.763
11.35
3.335
5.117
$R = 2$
9.828
3.335
5.104
$R = 1$
9.911
3.334
5.078
$R = 0$
4 6 8 10 12 14 16 18 20 22 24 26 28 30
Cu$K\alpha$ 2θ, deg
(b)
$W_{Mc} : W_{Sm} = 0.86 : 0.14$
9.668
15.95
11.37
3.336
5.136
$R = 3$
9.694
3.336
5.138
$R = 2$
11.64
9.762
3.336
5.129
$R = 1$
13.04
9.874
3.336
5.062
$R = 0$
$W_{Mc} : W_{Sm} = 0.84 : 0.16$
9.613
15.83
11.46
3.337
5.151
4.775
$R = 3$
9.631
3.337
5.156
$R = 2$
11.77
9.695
3.337
5.152
$R = 1$
13.0
9.834
3.338
5.117
$R = 0$
4 6 8 10 12 14 16 18 20 22 24 26 28 30
Cu$K\alpha$ 2θ, deg

nated with the maximum possible degree of order at $R = 2$, contain the low-angle reflection even at $W_{Sm} \geq 0.12$ but already with $d = 11.35–11.93$ Å (Figs. 3a–3c). At last, diffraction patterns of the Mc–Sm structures, in which layers of different types with $W_{Sm} \geq 0.14$ are alternated with the maximum possible degree of order at $R = 3$, contain already two low-angle reflections with $d = 11.37–11.60$ Å and 15.58–15.95 Å. Note that only one additional peak with $d = 11.23$ Å is observed in the low-angle region at $W_{Sm} = 0.12$ and $R = 3$.

The above analysis revealed two groups of diffraction patterns: with and without additional (as compared to "micaceous") reflections. Below, we shall consider only the mixed-layer Mc–Sm structures with $W_{Sm} \leq 0.20$ and $R = 0$ and with $W_{Sm} \leq 0.14$ and $R = 1$ which show no additional basal reflections in the low-angle region. Natural samples, diffraction patterns of which contain additional low-angle reflections, include Mc–Sm structures with $W_{Sm} \geq 0.16$ and $R = 1$ and with $W_{Sm} \geq 0.14$ and $R \geq 2$ (Figs. 3b, 3c). Since alternating layers of these structures could have no maximum possible degree of ordering, their complete characteristics may be obtained by simulation of the corresponding experimental XRD patterns.

Determination of Full Width of the Diffraction Maximum at Half-thickness

As known, the profile of basal reflections is determined by the statistically average thickness of CSD. Let us assume that the thickness of CSD in the studied mixed-layer structures is constant and equals $T = 9d(001)_{Mc} = 89.82$ Å regardless of the content of smectite layers. In this case,

$$T = N(9.98W_{Mc} + 16.85W_{Sm}), \quad (2)$$

where N is the average number of micaceous and smectite layers in the analyzed structure, and the terms $9.98W_{Mc}N$ and $16.85W_{Sm}N$ are contributions of thickness of the micaceous and smectite components, respectively, to the average thickness of CSD. Thus, if the relative contents of micaceous and smectite layers are W_{Mc} and W_{Sm}, respectively, the average number of layers in the CSD equals $N = T/(9.98W_{Mc} + 16.85W_{Sm})$. For instance, Mc–Sm structure with $W_{Mc} = 0.90$, $W_{Sm} = 0.10$, and $T = 89.82$ is characterized by $N = 8.420$. Table 2 shows the N variations depending on the content of smectite layers in Mc–Sm structures, which are characterized by a constant CSD thickness T = 89.82 Å.

At the given CSD thickness, we calculated diffraction patterns corresponding to mixed-layer structures

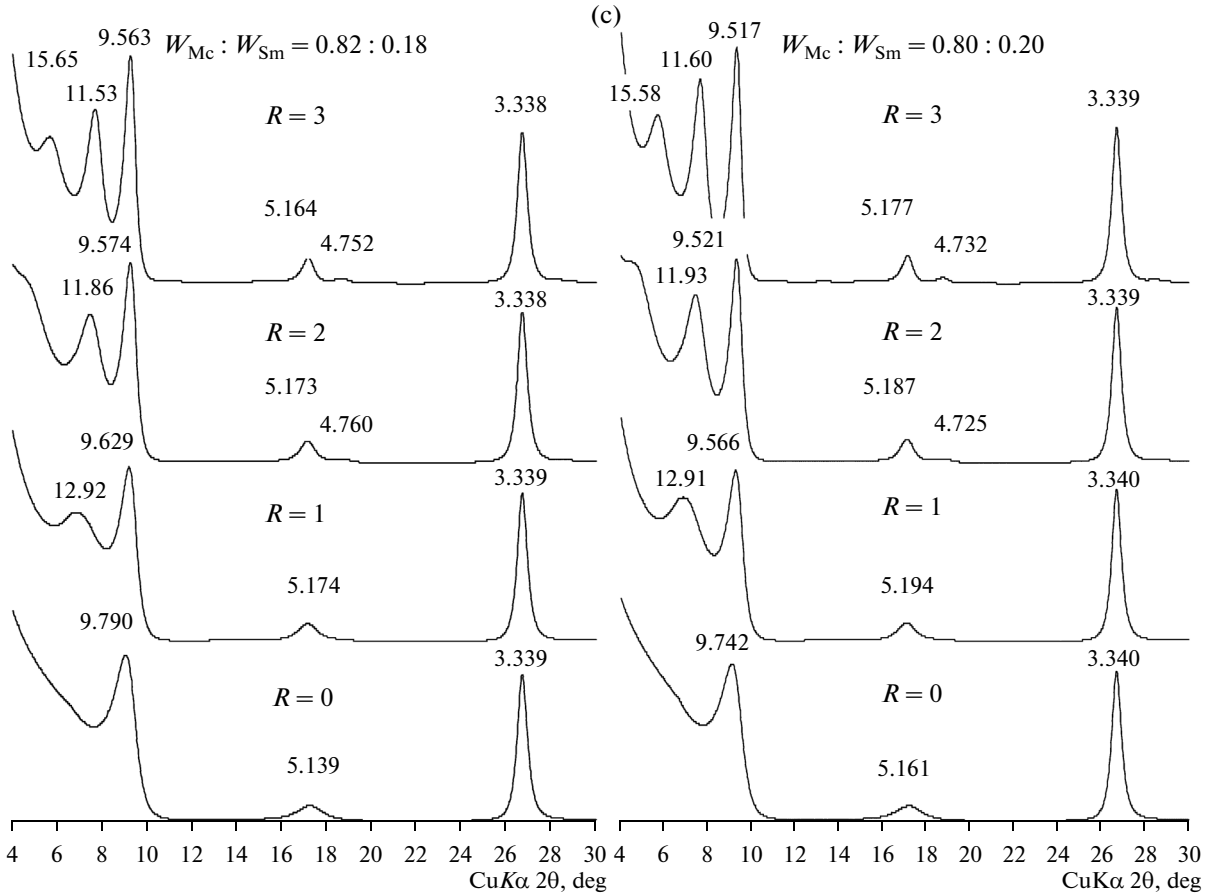

Fig. 3. Contd.

with $W_{Sm} \le 0.20$ at $R = 0$ and with $W_{Sm} \le 0.14$ at $R = 1$ and containing 12 orders of basal reflections. A successive increase of smectite layers in these structures was accomplished with a step of 0.02. From the calculated diffraction patterns, we excluded reflection 006 owing to its negligibly small intensity. Reflection 004 was excluded, because its asymmetrical shape did not allow us to accurately determine the true half-width. The remaining 10 orders of basal reflections corresponding to each of the analyzed Mc–Sm structures had sufficiently symmetrical shapes. Therefore, the width at half-thickness (half-width) of each reflection was determined by the direct measurement on a 2θ scale and was denoted as β (Fig. 4).

The half-widths of reflections were measured using Fytik software (Wojdyr, 2010). The Split-Pearson-VII analytical function was used to describe the profile of asymmetrical diffraction peak. The XRD pattern with the chosen 10 basal reflections was split preliminarily into individual segments containing one to three closely spaced basal reflections. For each distinguished segment of diffraction pattern, the background was subtracted as curve approximated by *n* degree polynomials. Then, each diffraction maximum in the distinguished region was specified by the symmetrical bell-shaped function, while the subsequent automated optimization provided the best fit between the calculated mathematical function and the experimental profile in the given region of diffraction curve. The degree of their correspondence was estimated visually from the difference curve. The values of half-width of reflection and its positions in 2θ angles were displayed on the screen (Fig. 4a).

Some problems arose during analysis of the low-angle reflection 001, the observed profile of which is distorted owing to the strong background scattering. Its intensity sharply increases toward low angles beginning from values 10°–11° 2θ, which mark the beginning of the record of intensity of the considered maximum. Distribution of the background scattering intensity was approximated by straight line, the slope of which was determined by profiles of the distribution of observed intensities adjacent to the analyzed reflection from the large and small 2θ angles (Fig. 4b). Successive subtraction of the background scattering intensity from the observed reflection profile in the distinguished 2θ region and application of the above-described optimization procedure provided the best fit between the calculated mathematical function and the "corrected" profile of 001 reflection.

In order to take into account the angular broadening of basal reflections caused by the relatively small thickness of CSDs, the obtained β values were multiplied by cosθ. Thus corrected half-width values (βcosθ) of reflections of different orders of a certain Mc–Sm structure were used to plot *Q* versus βcosθ curves.

Table 2. Average number of layers (*N*) in the mixed-layer Mc–Sm crystals of similar thickness T (89.92 Å) with alternating 9.98 Å micaceous and 16.85 Å smectite layers depending on the content of smectite layers (W_{Sm})

W_{Sm}, %	*N*
0	9.000
2	8.878
4	8.759
6	8.643
8	8.530
10	8.420
12	8.313
14	8.209
16	8.107
18	8.008
20	7.911
22	7.816
24	7.724

Dependence of Q on βcos θ for Mixed-layer Structures at R = 0

Required dependences were obtained using *Q* values corresponding to each index l_A of the observed basal reflections (Table 1). For each structure with the given W_{Sm}, half-widths of the observed 00*l* reflections (βcosθ) were determined by analyzing their optimized profiles. As expected, the values *Q* are well correlated with βcosθ at low contents of smectite layers ($W_{Sm} \le$ 10%) (Fig. 5a). Actually, correlation coefficients (R^2) characterizing the linear regressions between *Q* and βcosθ have high values and vary within a narrow range from 0.986 to 0.960 with variations in W_{Sm}. However, growth of W_{Sm} is accompanied by the subsequent deviation from linear dependence of reflections 001, 002, and 0012 owing to the decrease of corresponding βcosθ. On the contrary, deviation of reflections 003 and 0010 from the linear dependence is caused by increase of the corresponding βcosθ (Fig. 5b). It appeared that these deviations in the position of 00*l* reflections observed for each mixed-layer structure with different W_{Sm} are regular at all $W_{Sm} \le 0.20$ and with $R^2 \ge 0.995$ are described by cubic regression equations shown by dashed lines in Figs. 5a, 5b.

It should be emphasized that all regression equations corresponding to mixed-layer structures with $W_{Sm} \le 0.20$ and $R = 0$ have the same βcosθ value coinciding with the position of reflection 003 (Figs. 5a, 5b). Let us remind that mixed-layer structures with $W_{Sm} \le$ 0.20 and $R = 0$, for which diffraction patterns were calculated, had the same average thickness of CSD. This denotes that the position of reflection 003 for the two-component Mc–Sm structure with $R = 0$ in the plot of *Q* dependence on βcosθ is determined by the thickness of CSDs.

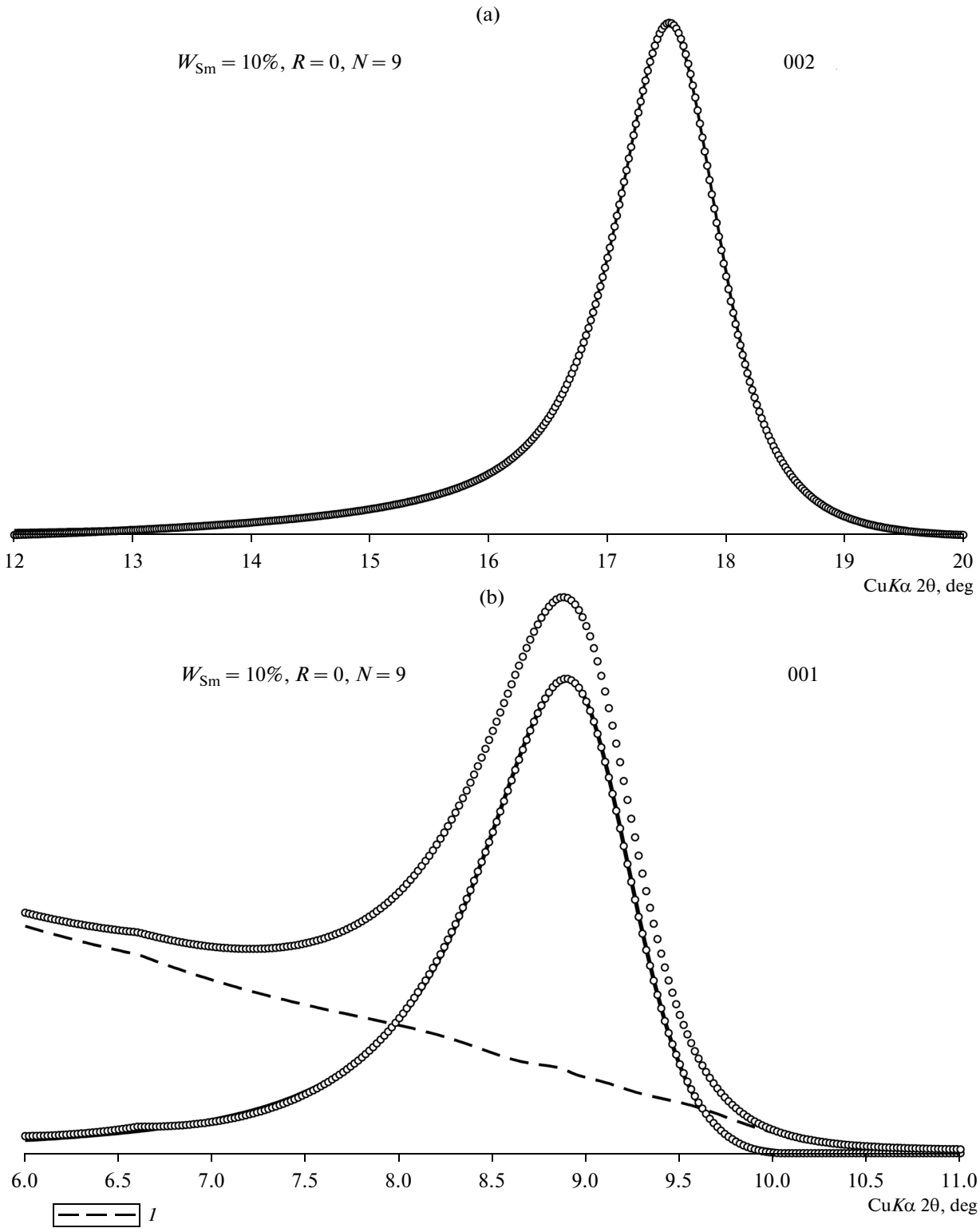

Fig. 4. Approximation of profiles of the diffraction maxima of reflections 002 (a) and 001 (b) calculated for the disordered mixed-layer structure Mc–Sm with $W_{Sm} = 10\%$ using Split–Pearson-VII function given in Fityk software (Wodjdyr, 2010). (*1*) Background scattering, intensity of which was subtracted from the analyzed profile.

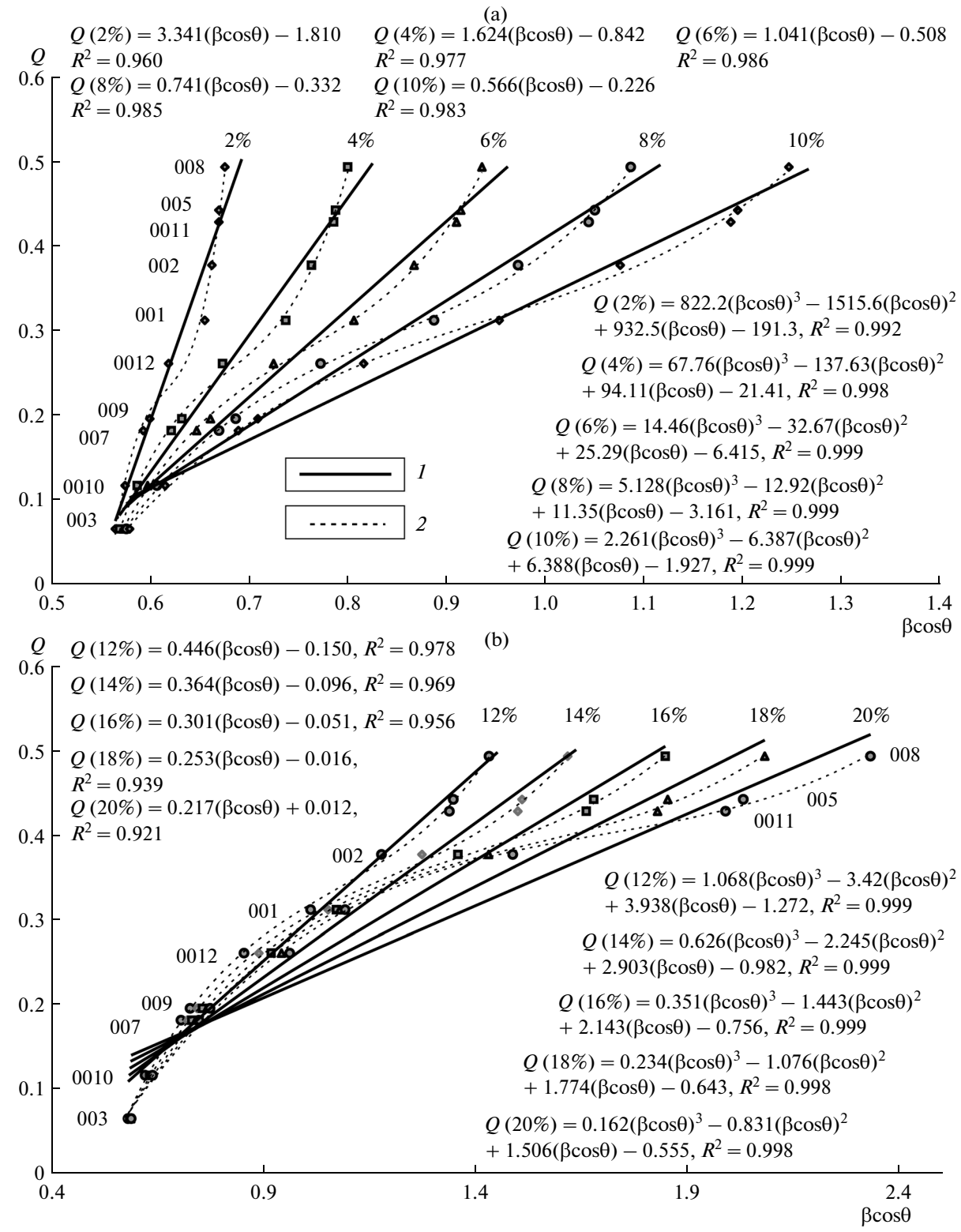

Fig. 5. Dependence of Q on $\beta\cos\theta$ for the disordered mixed-layer structures Mc–Sm calculated at W_{Sm} equal to 2–10% (a) and 12–20% (b). Lines corresponding to (*1*) linear and (*2*) cubic regression equations, which describe the position of the corresponding reflections in the plot at fixed W_{Sm} value.

Table 3. Values of slope angles (α) of straight lines described by the linear regression equations of Q dependence on $\beta\cos\theta$ for the mixed-layer structures made up of alternating mica (Mc) and smectite (Sm) layers 9.98 and 16.85 Å thicknesses with factors $R = 0$ and $R = 1$ at different W_{Sm}

W_{Sm}, %	α, deg		$\lvert\Delta W_{Sm}\rvert$, %	α, deg		$\lvert\Delta W_{Sm}\rvert$, %
	$R = 0$ (001–0012)	$R = 0$ (001–008)		$R = 1$ (001–0012)	$R = 1$ (001–008)	
2	73.3	73.6	0.01	72.6	73.0	0.23
4	58.4	59.2	0.06	55.6	56.7	0.15
6	46.2	47.3	0.04	41.7	43.1	0.07
8	36.5	37.8	0.05	29.9	32.2	0.15
10	29.5	30.7	0.03	23.3	24.2	0.03
12	24.0	25.1	0.04	18.0	18.3	0.01
14	20.0	21.0	0.11	14.2	14.0	0.00
16	16.7	17.4	0.05	–	–	–
18	14.2	14.6	0.06	–	–	–
20	12.5	12.5	0.06	–	–	–

Intervals of basal reflections with different indices 00*l*, which were used for plotting regression curves are shown in parentheses.
Values $\lvert\Delta W_{Sm}\rvert$ represent the difference of W_{Sm} values calculated from the cubic regression equations for reflections 001–0012 and 001–008, respectively.

Determination Of W_{Sm} Values From The Q Versus $\beta\cos\theta$ Straight Lines Slope

In spite of the fact that cubic regression equations reproduce with a higher accuracy the position of reflections 00*l* corresponding to the mixed-layer structure with each given W_{Sm}, we failed to establish the direct relationship of these equations with the content of smectite layers in the corresponding structure. The successive decrease of slope of straight lines relating Q and $\beta\cos\theta$ with W_{Sm} (Figs. 5a, 5b) may be applied to determine the content of smectite layers in the analyzed structures. It is shown that the value a in linear regression equations $y = ax + b$ determines $\tan\alpha$, where α is the slope angle of straight lines described by these equations to x axis. Thus, linear regression equations deduced for ten mixed-layer structures with different W_{Sm} were used to determine angles α corresponding to definite W_{Sm} (Table 3). Dependence of W_{Sm} on α shown in Fig. 6 is again described by regression equation

$$W_{Sm} = -0.0001\alpha^3 + 0.0202\alpha^2 - 1.2396\alpha + 31.925 \text{ with } R^2 = 0.998. \quad (3)$$

Variations of W_{Sm} versus α show that the accuracy of W_{Sm} determination decreases with increase of its value. For instance, if α values were determined accurate to 3°–5°, this value within the range of W_{Sm} from 2 to 8% may be determined with accuracy more than 0.5%. At such accuracy of α determination, W_{Sm} within the range of 16–20% could be determined with variations ±2%. Possible modifications of straight line's slopes depending on CSD thickness should be taken into account in practical application of obtained relationships.

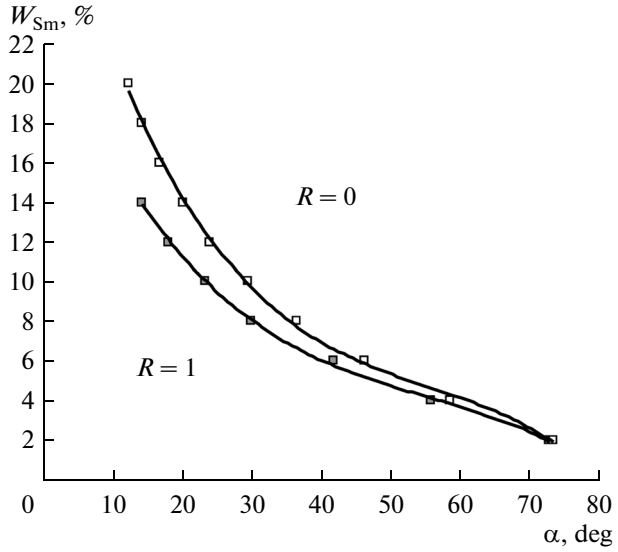

Fig. 6. Dependence of W_{Sm} on slope angle α at $R = 0$ and $R = 1$.

Determination of CSD Thickness

According to Mering's model, smectite reflection 005 with $d(005) = 3.37$ Å almost completely coincides with the mica reflection 003 with $d(003) = 3.327$ Å in

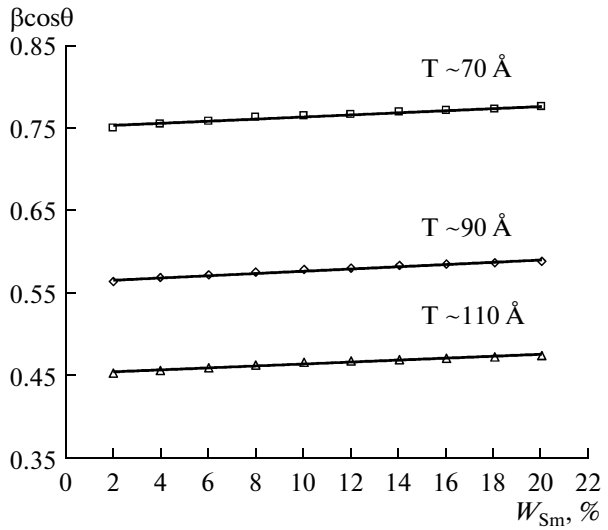

Fig. 7. Dependence of half-widths βcosθ corresponding to reflections 003 on W_{Sm} for the mixed-layer structures Mc–Sm at $R = 0$ and different values of T.

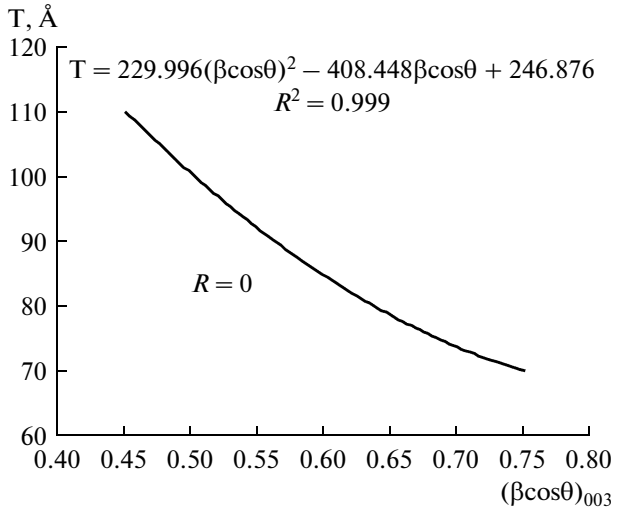

Fig. 8. Correlation between averaged thickness of crystals (T) and half-width $(\beta\cos\theta)_{003}$ of reflection 003.

two-component structures consisting of alternating 9.98 Å micaceous and 16.85 Å smectite layers (Fig. 1). This denotes that the half-width of reflection 003 also weakly depends on proportions of 9.98 Å and 16.85 Å layers in the mixed-layer structure, being mainly defined by the average thickness of the CSDs of crystallites. For this reason, all regression curves in Figs. 5a and 5b converge at one point, which coincides with reflection 003. Validity of these considerations is confirmed by the fact that dependences of βcosθ values, which correspond to reflections 003, on W_{Sm} calculated for mixed-layer structures with different T values represent a series of parallel straight lines (Fig. 7). Owing to small variations in βcosθ within ± 0.02, each curve may be approximated by linear regression almost parallel to *x* axis. Such approximation made it possible to establish the correlation between averaged CSD thickness (T) and half-width βcosθ of experimental reflection 003 (Fig. 8). This dependence is described by quadratic regression equation:

$$T = 229.996(\beta\cos\theta)^2 - 408.448\beta\cos\theta + 246.876 \text{ c } R^2 = 0.999. \quad (4)$$

Thus, βcosθ value of reflection 003 determines the average thickness T, while formula (2) may be used to calculate the average number of layers (*N*) in the studied structure at the known content of smectite layers (W_{Sm}).

Influence of CSD Thickness on the Accuracy of W_{Sm} Determination

It is very important from practical viewpoint to estimate the influence of T value on the slope of straight lines characterizing *Q* dependence on βcosθ, because this estimate defines the accuracy of W_{Sm} determination. Actually, the dependences of *Q* on βcosθ and W_{Sm} on α were calculated for fixed value T = 89.82 Å. If slopes of lines shown in Figs. 5a and 5b will depend on T, each T requires the corresponding series of *Q* versus βcosθ and W_{Sm} versus α.

In order to solve the set problem, we calculated diffraction patterns of structures with different W_{Sm} and T, determined βcosθ for the observed reflections 00*l*, and plotted *Q* versus βcosθ for each structure with the given W_{Sm} and T. In particular, Fig. 9 demonstrates a series of curves, which characterize the dependences of *Q* on βcosθ and correspond to mixed-layer structures with $W_{Sm} = 0.10$, but with different T values (69.86, 79.84, 89.82, 99.80, 109.78, and 119.76 Å). Regression equation obtained for each straight line was used to determine its slope angle (α) corresponding to each T value. Values of angles 28.8° and 28.0° corresponding to T = 69.86 and 109.78 Å, respectively, differ from angle α = 28.5° calculated at T = 89.82 Å by only 0.5°. This denotes that *Q* versus βcosθ plots calculated for mixed-layer structures with the given content W_{Sm} and different T remain practically parallel to each other, and errors in W_{Sm} determination are no more than tenths of percent.

Similar result was obtained by the comparison of *Q* versus βcosθ curves characterizing the distribution of positions of reflections 00*l* using the cubic regression equations (Fig. 9). As in the previous case, the profiles of curves with similar W_{Sm} but different T were very close.

Mixed-layer Mc–Sm Structures with $W_{Sm} \le 0.14$ and $R = 1$. Dependence of Q on T

As shown above, diffraction patterns of the ethylene glycol-saturated Mc–Sm structures with $W_{Sm} >$

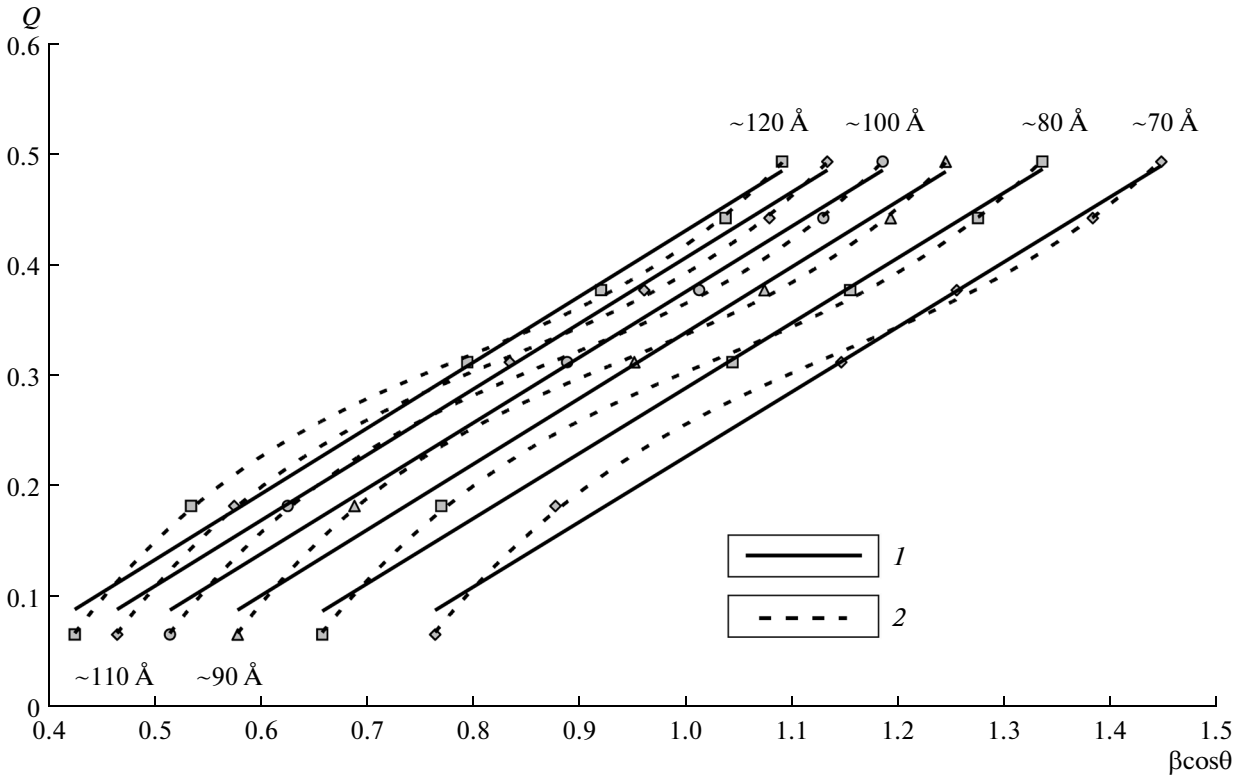

Fig. 9. Dependence of Q on $\beta\cos\theta$ corresponding to the mixed-layer Mc–Sm structures with content $W_S = 0.10$, but different crystal thickness (T) values and described by linear (*1*) and cubic (*2*) regression equations.

0.14 and $R = 1$ show low-angle reflections with $d \leq 13.0$ Å. Therefore, the corresponding experimental XRD pattern must be simulated to determine reliably the probability parameters controlling the distribution of alternating layers in the analyzed structure. On the basis of analysis of relationships between half-widths of basal reflections and corresponding Q values, we attempted to determine the amount of smectite layers and their distribution in structures with $W_{Sm} \leq 0.14$ and $R = 1$. To solve this problem, we calculated diffraction patterns containing the basal reflections of mixed-layer structures, in which layer pairs 26.83 Å are randomly alternated with 9.98 Å micaceous layers. In such structure, smectite 16.85 Å layers are separated from each other by at least one micaceous layer. Hence, micaceous and smectite layers are alternated with factor $R = 1$. As for the case described above, it was suggested that the CSD thickness (T) is similar for structures with different W_{Sm} and equal 89.82 Å. The Q values for basal reflections with different indices 00l have similar values for structures with $R = 0$ and $R = 1$ (Table 1). Profiles and half-widths of basal reflections with different l were determined using the same procedure as that for the determination of $\beta\cos\theta$ for structures with $R = 0$. It was found that the shape of Q variations versus $\beta\cos\theta$ depending on W_{Sm} is similar for structures with $R = 0$ and $R = 1$. As in the case with $R = 0$, the distribution of basal reflections 00l that are defined by Q dependence on $\beta\cos\theta$ is described at each given W_{Sm} within the range $0.02 < W_{Sm} < 0.14$ with $R^2 \geq 0.99$ by cubic regression equations (Figs. 10a, 10b). At the same time, at $W_{Sm} \leq 0.08$, the distribution of observed basal reflections determinable at each given W_{Sm} by Q dependence on $\beta\cos\theta$ may be described by linear regression equation with $R^2 = 0.96–0.98$ (Fig. 10a). Further increase of W_{Sm} from 0.08 to 0.14 is accompanied by even more significant deviation of some basal reflections from positions described by linear dependence. In particular, the values $\beta\cos\theta$ corresponding to the reflections with indices 001, 002, and 0012 successively decrease, while those corresponding to reflections 003 and 008 increase. As in the case with $R = 0$, each linear regression equation at the given W_{Sm} was used to determine the slope angle of the corresponding straight line with respect to axis x. Calculations showed that the straight lines characterizing Q dependence on $\beta\cos\theta$ and corresponding to mixed-layer structures with the given W_{Sm} but different T are parallel to each other. This denotes that variations of W_{Sm} versus α (Fig. 6) described by regression equation

$$W_{Sm} = -0.0001\alpha^3 + 0.0133\alpha^2 - 0.8337\alpha + 23.2806, \quad (5)$$

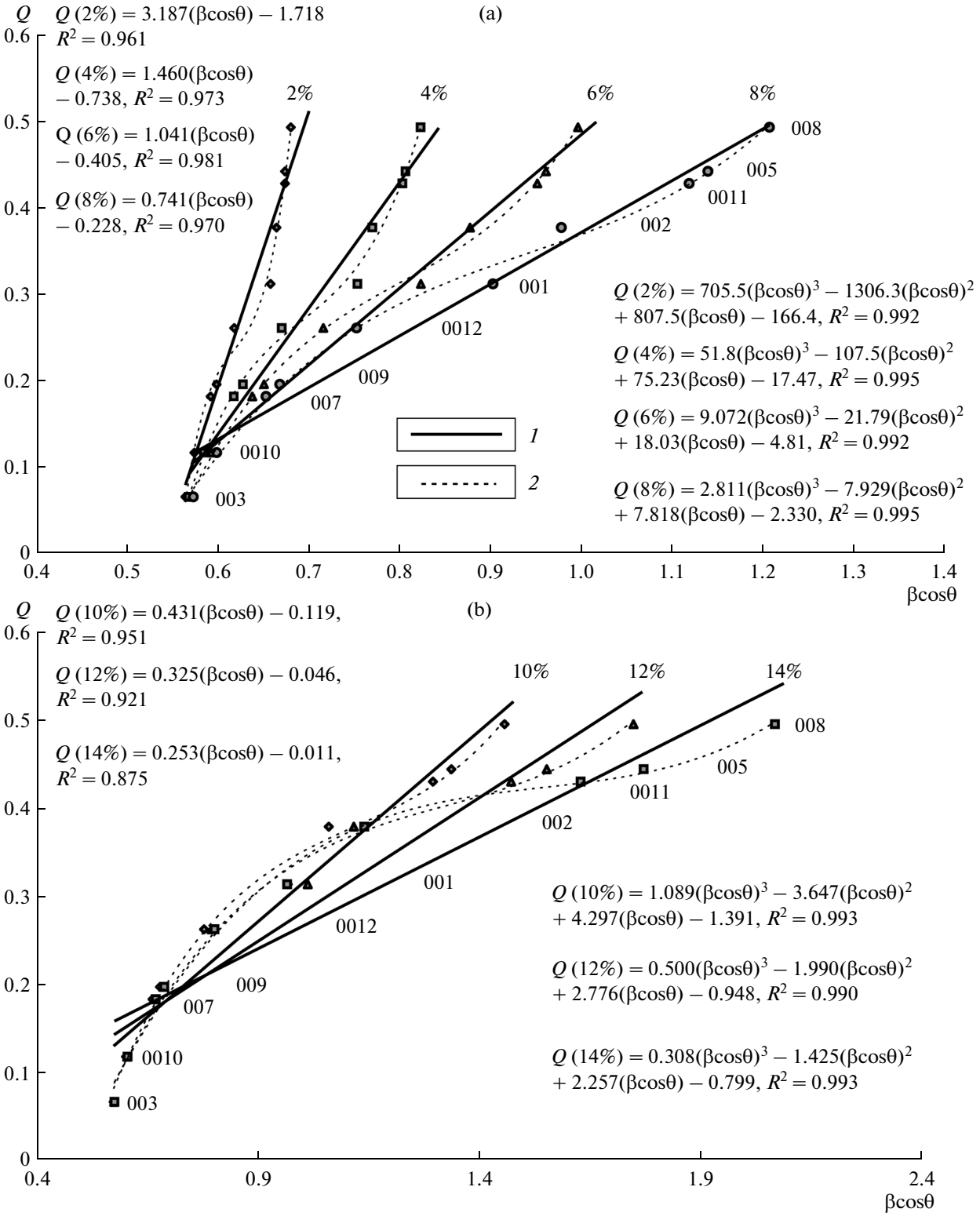

Fig. 10. Dependence of Q on the $\beta\cos\theta$ for the mixed-layer Mc–Sm structures calculated at W_{Sm} equal to 2–8% (a) and 10–14% (b) at $R = 1$. Lines corresponding to the (*1*) linear and (*2*) cubic regression equations describing the position of the corresponding reflections in the plot at fixed W_{Sm}.

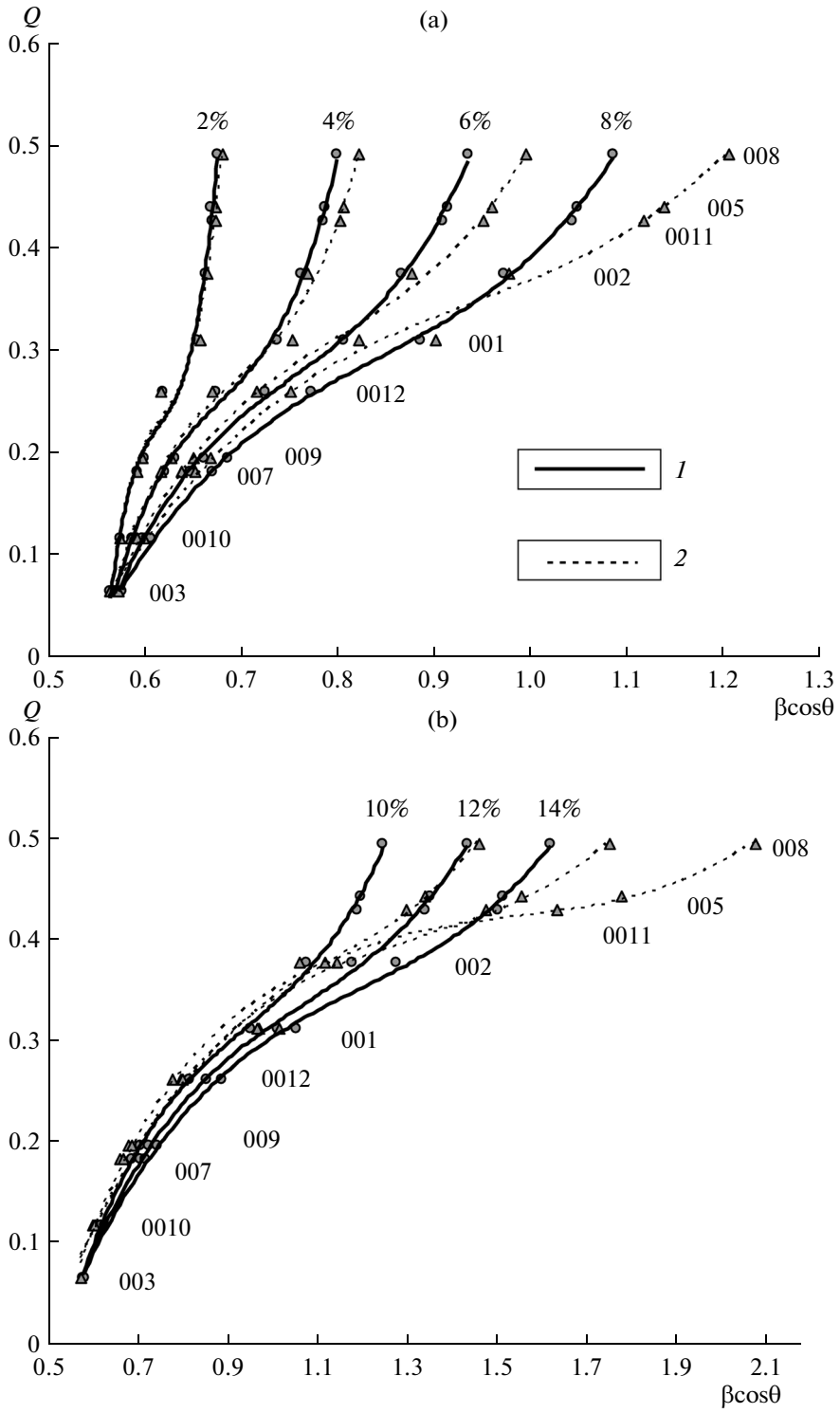

Fig. 11. Dependence of Q on $\beta\cos\theta$ for the mixed layer Mc–Sm structures, in which the content of smectite layers (W_{Sm}) varies from 2 to 8% (a) and from 10 to 14% (b), while their distribution corresponds to $R = 0$ (1) and $R = 1$ (2).

may be used for determination of the content of smectite layers in natural two-component structures, in which 9.98 Å micaceous and 16.85 Å smectite layers at $W_{Sm} \leq 0.14$ are alternated with $R = 1$.

Determination of the Short-Range Order Factor R

Figure 11 demonstrates curves characterizing Q dependence on $\beta\cos\theta$ for mixed-layer structures with identical contents of smectite layers but their different

distributions between micaceous layers, i.e., with $R = 0$ and $R = 1$. It is well seen that the largest differences between curves corresponding to $R = 0$ and $R = 1$ with increasing W_{Sm} are observed for the largest Q values, which sandwich reflections 005 and 008. The higher W_{Sm}, the more the difference between $\beta\cos\theta$ values for reflections 005 and 008 located on the curves with $R = 0$ and $R = 1$. At the same time, increase of W_{Sm} is accompanied by increase in difference between $\beta\cos\theta$ values corresponding to reflections 008 and 005 passing from the curve with $R = 0$ to the curve with $R = 1$. These features make it possible to distinguish the random alternation of different layers from the alternation with short-range order factor $R = 1$ for two-component mixed-layer structures with a low content of smectite layers. For this purpose, $\beta\cos\theta$ corresponding to reflection 003 should be subtracted from $\beta\cos\theta$ corresponding reflections 005 and 008 situated in the curves with $R = 0$ and $R = 1$ to avoid the influence of CSD thickness on the $\beta\cos\theta$ value of the considered reflections. At the next step, differences between the $\beta\cos\theta$ values corresponding to reflections 008 and 005 at each given W_{Sm} should be determined for all $W_{Sm} \le 0.14$, for which the Q dependence on $\beta\cos\theta$ was calculated at $R = 0$. This offers an opportunity to plot the dependence $\Delta_0 = (\beta\cos\theta)_{008} - (\beta\cos\theta)_{005}$ on W_{Sm} for mixed-layer structures with $R = 0$ and $W_{Sm} \le 0.14$. Similar procedure was used to determine the Δ_1 versus W_{Sm} dependence for mixed-layer structures with $R = 1$. Comparison of the obtained dependences (Fig. 12) indicates that the difference between Δ_0 and Δ_1 within W_{Sm} 8–14% at each W_{Sm} is large enough to distinguish the random distribution of smectite layers between micaceous layers from the distribution with tendency to maximum possible degree of ordering at $R = 1$ even at low contents of smectite layers.

Identification of Two-Component Mixed-Layer Structures with R = 0 and R = 1

During study of the finely dispersed dioctahedral micaceous samples containing smectite interlayers with $W_{Sm} \le 0.14$, the order of their alternation remains unknown if XRD patterns contain basal reflections, the number and position of which is the same as in monomineral 1M micas.

Under these conditions, the order of alternation of different types of layers in the studied structure may be determined using the following procedure:

(i) determination of the half-width of basal reflections $\beta(00l)$ recorded on the XRD pattern from the ethylene glycol sample and correction of the obtained $\beta(00l)$ for the corresponding values of $\cos\theta$;

(ii) approximation of Q dependence on $\beta\cos\theta$ by the linear regression equation to determine the slope angle α of the straight lines;

(iii) the obtained α may correspond to two W_{Sm} values determined from the dependences of W_{Sm} on α and corresponding to the distribution of different layers with $R = 0$ and $R = 1$ (Eqs. 3, 5);

(iv) determination of difference (Δ) between $\beta\cos\theta$ values corresponding to reflections 008 and 005 recorded on the experimental XRD pattern;

(v) determination of two values Δ_0 and Δ_1 for two W_{Sm} values corresponding to structures with $R = 0$ and $R = 1$ (Fig. 12); and

(vi) comparison of Δ_0 and Δ_1 with the experimentally determined Δ to determine the tendency prevailing in the distribution of smectite layers between micaceous layers in the studied sample.

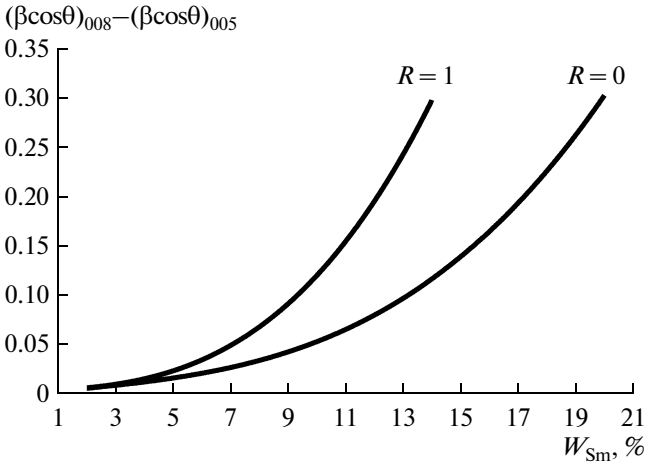

Fig. 12. Dependence of $[(\beta\cos\theta)_{008} - (\beta\cos\theta)_{005}]$ on W_{Sm} for the mixed-layer structures with $R = 0$ and $R = 1$.

EXPERIMENTAL

Choice of Reflections

Preliminary experience in obtaining XRD patterns from the oriented specimens of studied samples containing 12 orders of reflections showed that their record requires much time. It appeared that $00l$ reflections with $l \ge 9$ have a very low intensity, while long-term record may be accompanied by the partial evaporation of ethylene glycol molecules from expandable interlayers of the structure. For this reason, we decided to constrain the number of reflections in the experimental XRD patterns, omitting $00l$ reflections with $l \ge 9$ from consideration. In order to estimate errors, which could arise due to such limitation, we compared the slope angles α of straight lines described by linear regression equations, which include the half-width of $00l$ reflections from 001 to 0012 and from 001 to 008, respectively. Such a comparison was carried out for mixed-layer structures with $R = 0$ and $R = 1$ at different W_{Sm}. As follows from Table 3, difference in the comparable α values is systematic, i.e., α value at given W_{Sm} for a limited set of $00l$ reflections ($l \le 8$) is always 0.2°–1.4° higher than those for $00l$ reflections with $l \le 12$. Using formulas (3) and (5), W_{Sm} was calculated for

Table 4. Slope angles of straight lines (α) and structural parameters of the studied samples

Sample no	α, deg	W_{Sm}, %	T, Å	*N*
560/3	39.89	7.34	79.3	7.57
555A	40.95	7.06	78.64	7.51
60	30.98	9.80	87.28	8.19
555B	29.31	10.39	70.32	6.58
553/1	24.01	12.61	72.87	6.72
400/3	49.18	5.61	76.43	7.37
402/1	41.90	6.92	74.68	7.14
37/71	48.54	5.71	72.52	6.99
RM30	51.06	5.34	124.67	12.05

W_{Sm} is the content of smectite layers, T is the average thickness of mixed- layer crystals, *N* is the average number of layers in crystals.

each pair of α values. This procedure allowed us to estimate ΔW_{Sm}, which should be added to each W_{Sm} determined at the given *R* factor and limited number of basal reflections. This addition, on average, varies from 0.01 to 0.11%, i.e., has a negligibly small value (Table 3).

Determination of the Half-Width of Experimental Reflections

One of important requirements to the quality of analyzed reflection consisted in obtaining a large number of X-ray impulses characterizing its profile. In other aspects, procedure of the determination of reflection width at its half-thickness was similar to the procedure described above for reflections in the calculated diffraction patterns. Experimental XRD patterns were subdivided into two or three segments with closely spaced basal reflections. For each segment, the background line was subtracted, and each reflection was described by the bell-shaped function, while automated optimization performed using Fytik software provided the best fit of experimental profile of analyzed reflection and calculated function. While multiplying the obtained β value by the corresponding cosθ value, we took into account the dependence of angular broadening of the basal reflection owing to the small thickness of CSDs.

Determination of the Contents of Smectite Layers

Experimental values $(\beta\cos\theta)_e$ corresponding to the above-described limited number of 00*l* reflections ($l \leq 8$) were used to plot *Q* dependence on $(\beta\cos\theta)_e$ for each of the studied samples. In general, positions of 00*l* reflections shown in Figs. 13a–13c by dark circles are described by the linear regression equations with *R*-factor varying in different samples from 0.85 to 0.99. Straight lines shown in Figs. 13a–13c by solid lines correspond to regression equations, which are located at the top left corner of the plots. The slope angles (α) of straight lines were used to calculate the content of smectite layers (W_{Sm}) in each sample using Eq. (3). As seen from Table 4, W_{Sm} in structures of the studied micaceous varieties varies from 5.3 to 12.6%.

Note one peculiarity in the distribution of half-widths $(\beta\cos\theta)_e$ corresponding to reflections with index 002. For instance, mixed-layer structures of samples 555A and 560/3 contain close W_{Sm} values (7.1 and 7.3%, respectively). At the same time, as seen from Fig. 13a, the deviations of positions $(\beta\cos\theta)_e$ corresponding to different reflections 00*l* of sample 555A relative to the regression line are sufficiently evenly distributed. The values of $(\beta\cos\theta)_e$ of all reflections of sample 560/3 also plot near the regression straight line, except for the half-width $(\beta\cos\theta)_e$ corresponding to reflection 002. We could not reveal structural features of this sample responsible for such sharp deviation of its experimental half-width from the predicted value. Since slopes of the straight lines corresponding to samples 555A and 560/3 seemed to be practically identical, it is logical to conclude that sharp deviation of the half-width $(\beta\cos\theta)_e$ of reflection 002 from the regression straight line observed for sample 560/3 was not caused by the incorrect determination of the number of smectite layers, but is related with other yet unknown causes. Distribution of $(\beta\cos\theta)$ in the plots showing variations of *Q* versus $(\beta\cos\theta)_e$ makes it possible to divide the samples into two groups. In one group, the half-widths $(\beta\cos\theta)_e$ of all 00*l* reflections are sufficiently evenly distributed relative to the regression straight lines (samples 555A, 37/71, 400/3, RM30, 553/1). In another group, the position $(\beta\cos\theta)_e$ of reflection 002 is sharply shifted to the left relative to its predicted position in the regression straight line, which is attributed to the much narrower experimental half-width of this reflection (samples 555B, 560/3, 402/1, 60) (Figs. 13a–13c).

DISCUSSION

Simulation of XRD Diffraction Patterns

One of the best ways to test the correspondence of W_{Sm} determined by analyzing the half-widths of basal reflections to the true content of smectite layers in the structure of studied samples consists in the simulation of XRD patterns of structural models, the parameters of which include proportions of micaceous and smectite layers ($W_{Mc} : W_{Sm}$), as well as the thickness of the coherent scattering domains (T) determined from experimental XRD patterns. The T value of each sample was determined using formula (4), which describes relationships between the average CSD thickness and half-width βcosθ of experimentally observed profile of reflection 003 (Table 4). As already mentioned, the half-width of this reflection practically does not depend on the content of smectite layers in the structure of the studied sample. The W_{Sm} values and CSD thickness were used to determine the average number of layers (*N*) in the averaged CSD of the studied struc-

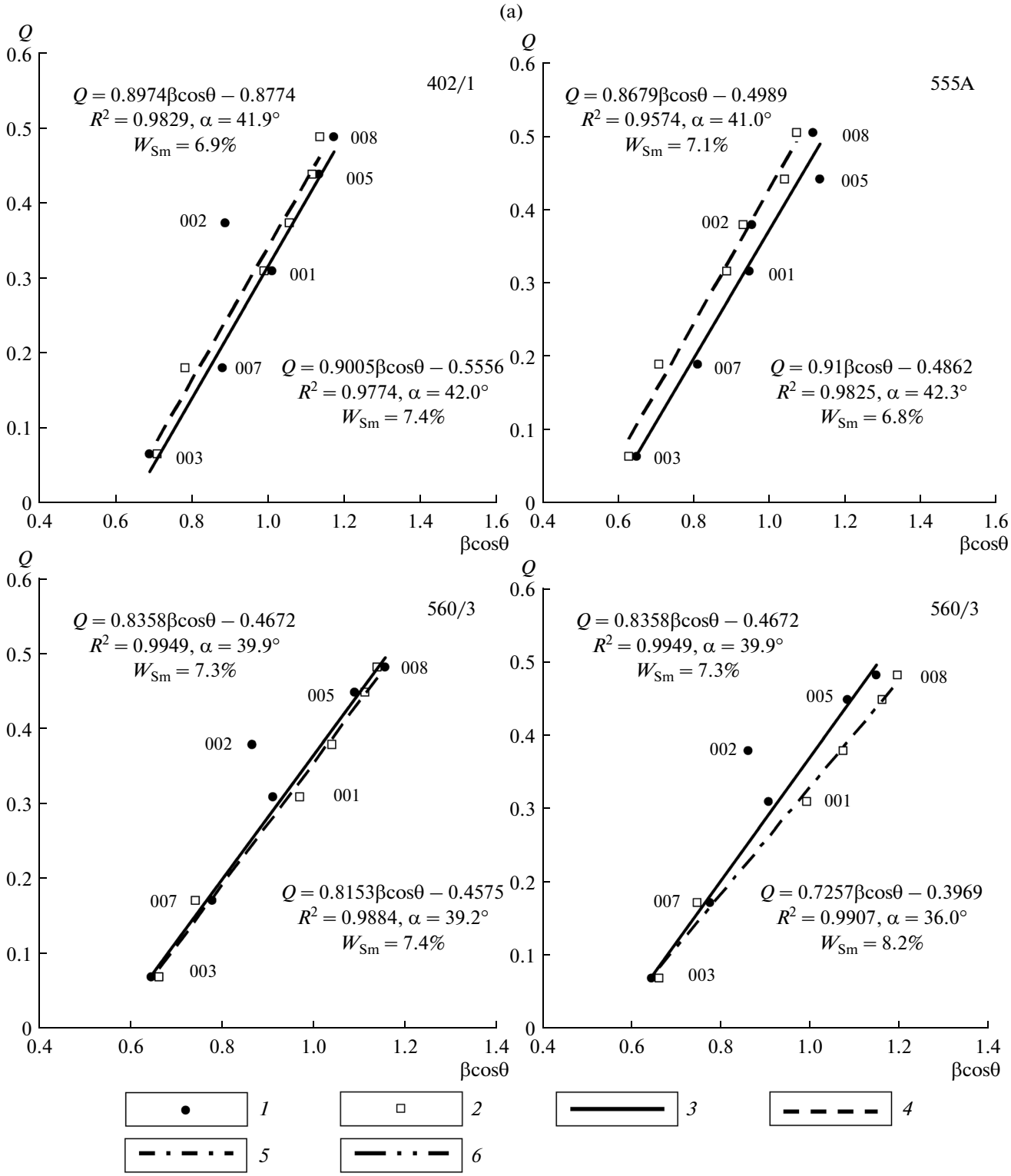

Fig. 13. Dependence of Q on $\beta\cos\theta$ for the studied samples: (a) 402/1, 555A, 560/3; (b) 400/3, 37/71, RM30; (c) 555B, 60, 553/1. (*1*) Experimental and (*2*) calculated half-widths of basal reflections: regression straight lines corresponding to the (*3*) experimental and (*4*) calculated half-widths of reflections: (*5*) regression straight line for sample 560/3 corresponds to the distribution of half-widths of reflections calculated at $W_{Sm} = 8.3\%$; (*6*) regression straight lines for samples 400/3 and 555B correspond to the distribution of half-widths of basal reflections calculated for the mixed-layer structures with variations of the thickness of micaceous layers with standard deviation $\Delta\xi = 0.06$ Å. The regression equations and W_{Sm} corresponding to the experimental and calculated straight lines and the contents of smectite layers are shown in the top left and bottom right.

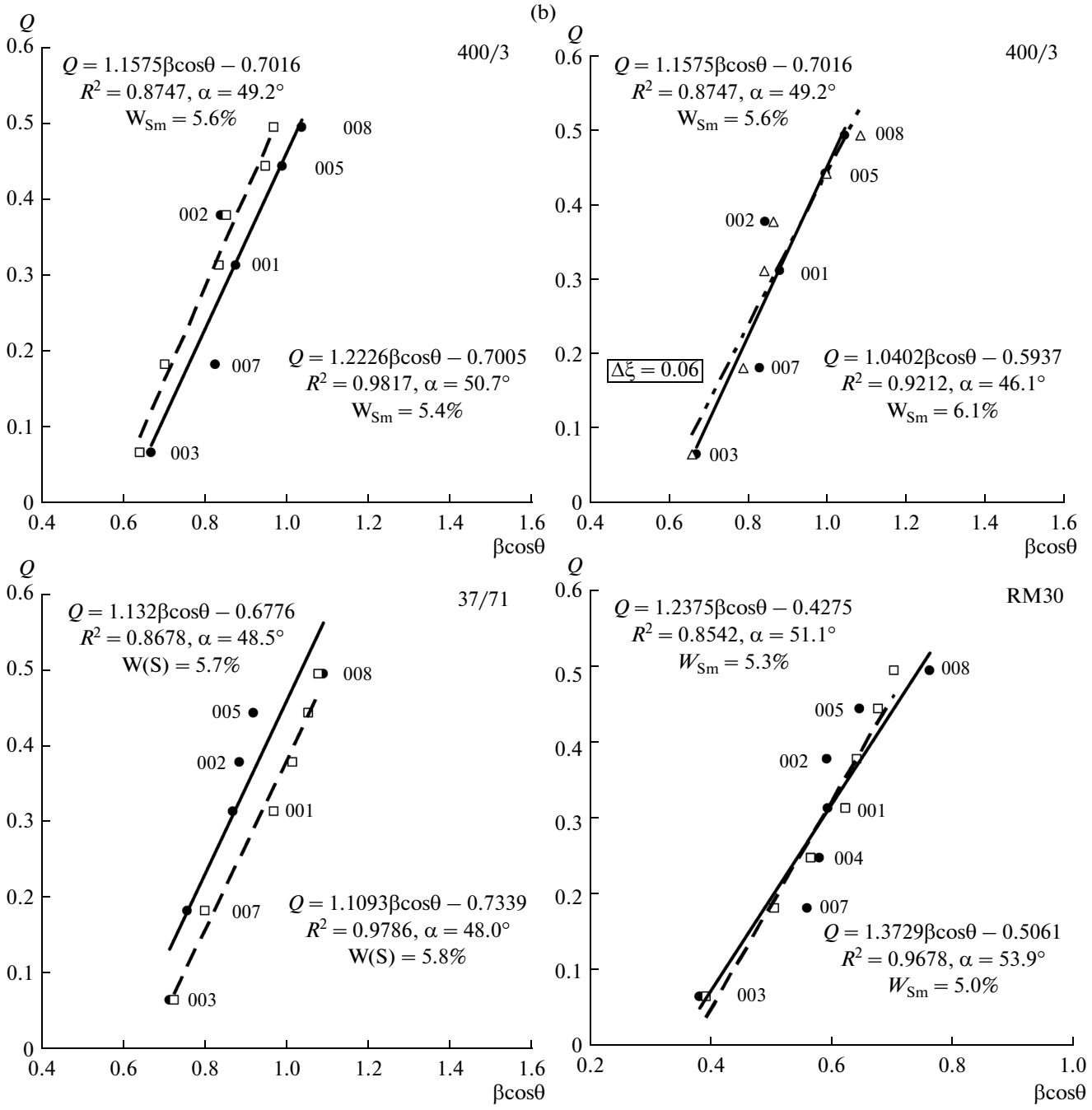

Fig. 13. Contd.

tures using formula (2) (Table 4). Distribution of cations over the structural sites of octahedral and tetrahedral sheets of 2 : 1 layers and interlayers of micaceous and smectite layers was given on the basis of structural formula of the studied samples presented in (Ivanovskaya et al., 2012; Drits et al., 2010).

Thus, the XRD patterns of each sample were simulated using the cation composition, content, distribution ($R = 0$), and thicknesses of different layers, thickness T, and number of layers in the averaged CSD of the studied structure. As seen in Figs.14a–14c, the calculated diffraction patterns satisfactorily reproduce the main features of experimental XRD patterns. It is known that the main diffraction characteristic of mixed-layer structures is the presence of nonrational series of corresponding basal reflections. The fact that the positions of reflections in the comparable XRD patterns corresponding to samples with different contents of smectite layers practically coincide may be considered as evidence for very close or even identical

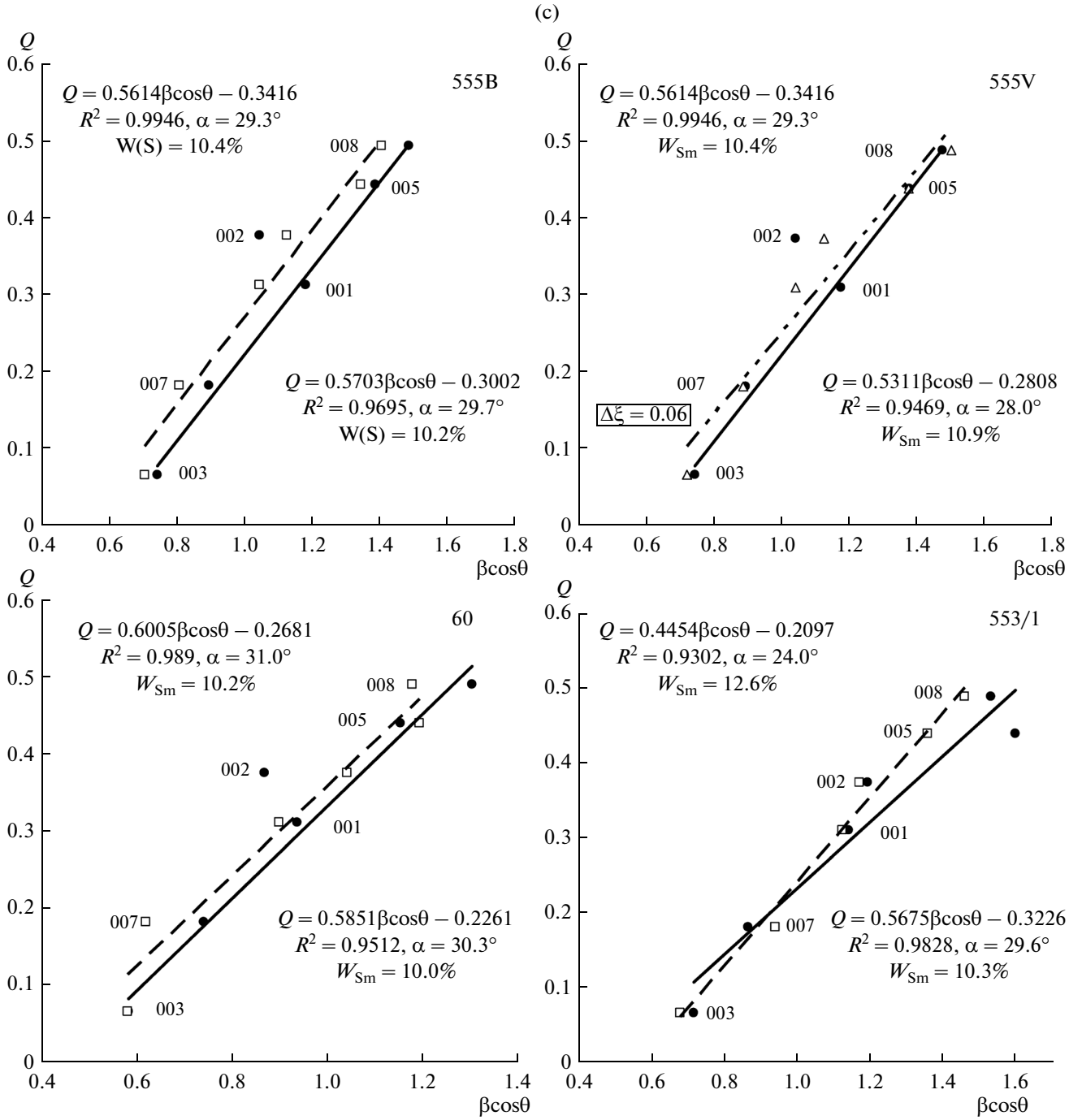

Fig. 13. Contd.

contents of smectite layers in the models and studied samples. Moreover, the intensities of reflections with similar 00*l* indices in the comparable diffraction patterns usually have very close values (Figs. 14a–14c). Exceptions are calculated and experimental intensities of reflections 005 (sample 560/3) and 007 (samples 555B, 60). Note that the comparable patterns of all samples, except sample RM30, demonstrate a strong experimental maximum against a weak calculated reflection 006. These differences are related to the insufficiently high degree of orientation of particles of globular samples. Actually, the observed experimental maxima in the given 2θ region were caused by the contribution of three-dimensional reflections with indices *h3l* in its intensity (Drits et al., 2010). Owing to the high degree of particle orientation in the specimen of sample RM30, its XRD pattern lacks *hkl* reflections, resulting in the coincidence of intensities of reflec-

tions 006 in the calculated and experimental patterns (Fig. 14b).

Comparison of $(\beta\cos\theta)_e$ and $(\beta\cos\theta)_c$

Profiles of basal reflections observed in the modeled diffraction patterns were optimized. This provided the exact determination of half-width β, angle 2θ, and, hence, $(\beta\cos\theta)_c$ of each analyzed maximum. As example, the mutual location of $(\beta\cos\theta)_e$ and $(\beta\cos\theta)_c$ values corresponding to basal reflections 00*l* of samples 555A and 560/3 is shown in Fig. 15. For sample 560/3, experimental $(\beta\cos\theta)_e$ and calculated $(\beta\cos\theta)_c$ halfwidths of all reflections 00*l* have very close values, except for reflection 002, the experimental half-width of which is much narrower than the calculated one. As already mentioned, we could not determine what caused the difference in the comparable half-widths of this reflection. In contrast, sample 555A demonstrates very close values of comparable half-widths for reflections with $l \le 3$, i.e., including half-widths of reflection 002. However, experimental half-widths of reflections with $l \ge 5$ seemed to be much wider than calculated ones. One of the possible reasons for the observed inconsistency is fluctuations of thicknesses of alternating layers, the presence of which leads to the broadening of basal reflections (Drits and Tchoubar, 1990).

It is noteworthy that even a comparatively small number of expandable layers in the mixed-layer Mc–Sm structure results in the contrasting distribution of half-widths of reflections 00*l* as compared to those of basal reflections of the periodical structure consisting of only mica layers (Fig. 15).

Peculiarities in the distribution of $(\beta\cos\theta)_e$ and $(\beta\cos\theta)_c$ depending on Q

In Figs. 13a–13c, which demonstrate the *Q* dependence on $(\beta\cos\theta)_c$ in the studied samples, one can see that straight lines characterizing the distribution of experimental and calculated half-widths of basal reflections are either practically coincident (samples 560/3, 402/1, RM30) or almost parallel to each other (samples 555A, 60, 37/71). In the last case, the difference of slope angles of the lines is usually less than 1°, while corresponding W_{Sm} values are no more than 0.2%. Even if the difference between α_e and α_c determined for slope angles of the comparable straight lines (sample RM30) is 2.8°, the content of smectite layers differed by only 0.3% (Fig. 13b).

Error in Determination of the Content of Smectite Interlayers, W_{Sm}

In order to reveal the difference between α_e and α_c, which provides the required accuracy in determination of W_{Sm} in the studied mixed-layer structures, XRD diffraction patterns were calculated for structural models, in which the content of smectite layers is 1% higher than W_{Mc} determined from the slope of experimental regression straight line. This is exemplified in Fig. 13a by the comparison of regression straight lines corresponding to the distribution of half-widths of experimental reflections for sample 560/3 and reflections calculated for the mixed-layer structure containing 8.3% smectite layers, i.e., 1% more than that established from the slope of experimental straight line (7.3%, sample 560/3). It is seen in the figure that an increase of W_{Sm} led to the decrease of slope angle of calculated regression straight line by 3.8° as compared to the slope angle of experimental straight line, which corresponds to $W_{Sm} = 8.2\%$. This example demonstrates that if comparable experimental and calculated straight lines are parallel to each other or inclined with respect to each other at 1 or 2°, accuracy of the calculated percentages of W_{Sm} is not higher than tenths of a percent.

Thus, the obtained results indicate that the described technique makes it possible to obtain reliable quantitative information for low contents of smectite layers ($W_{Sm} \le 10–12\%$) in the dispersed dioctahedral K-bearing illite and glauconite mineral varieties.

Effect of Variations of Micaceous Interlayer Thicknesses Relative to Their Average Value

Detailed analysis of the mutual position of $(\beta\cos\theta)_e$ and $(\beta\cos\theta)_c$ corresponding to reflections 005, 007, and 008 provides additional information on structural features of the studied samples. In particular, a distinctive feature of the distribution of $(\beta\cos\theta)_e$ and $(\beta\cos\theta)_c$ observed for samples 400/3 (Fig. 13b) and 555B (Fig. 13c) is the fact that the calculated half-widths of 005, 007, and 008 reflections are narrower than those of experimental ones. In order to understand the nature of this effect, we need to take into account one of the characteristic features of the dispersed dioctahedral 2 : 1 micaceous varieties: manifestation of wide isomorphism caused by the substitution of Si for Al in the tetrahedral sheets and the substitution of trivalent cations (Al, Fe^{3+}) for divalent ones (Mg, Fe^{2+}) in the octahedral sheets of 2 : 1 layers. These isomorphic substitutions may result in heterogeneity of the cationic composition of individual micro- and nanocrystals, which compose the sample,

Fig. 14. Experimental and calculated diffraction patterns for the studied samples: (a) 560/3, 555A, and 402/1; (b) 400/3, 37/71, and RM30; (c) 555B, 60, and 553/1. Comparison of fragments of the experimental and calculated diffraction patterns corresponding to the basal reflections 001 and 005 are shown for sample 553/1.

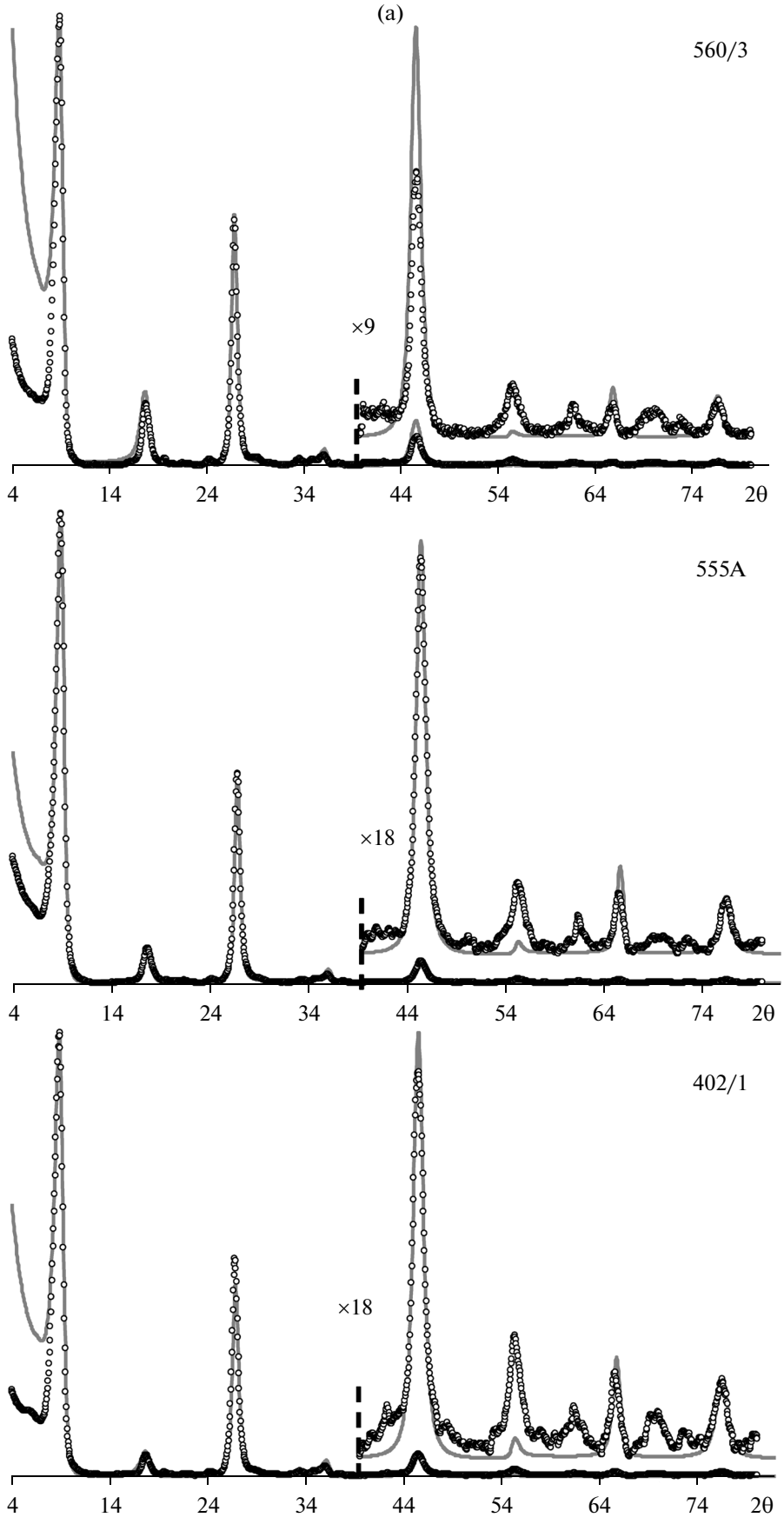
(a)
560/3
×9
4
14
24
34
44
54
64
74
2θ
555A
×18
4
14
24
34
44
54
64
74
2θ
402/1
×18
4
14
24
34
44
54
64
74
2θ

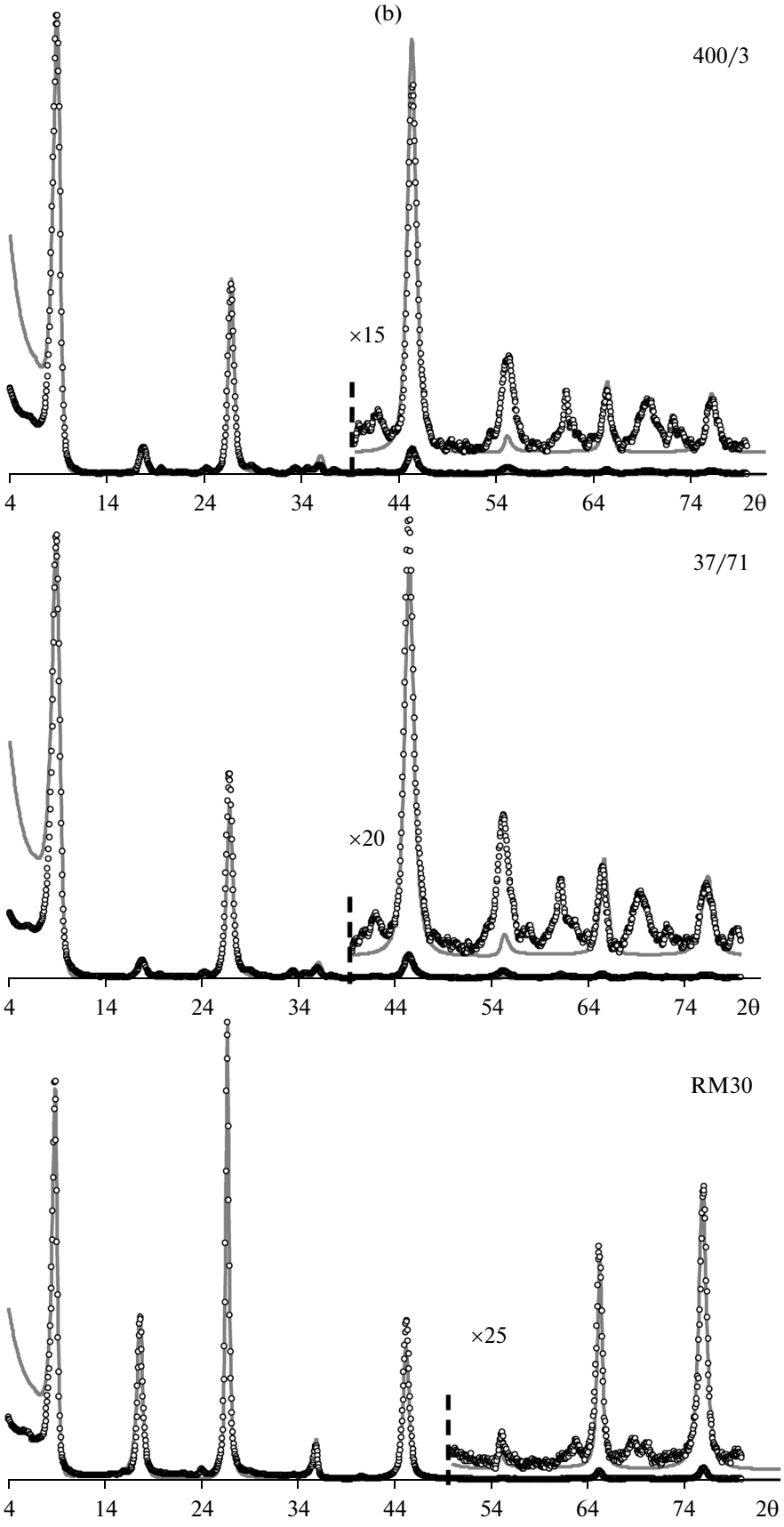

Fig. 14. Contd.

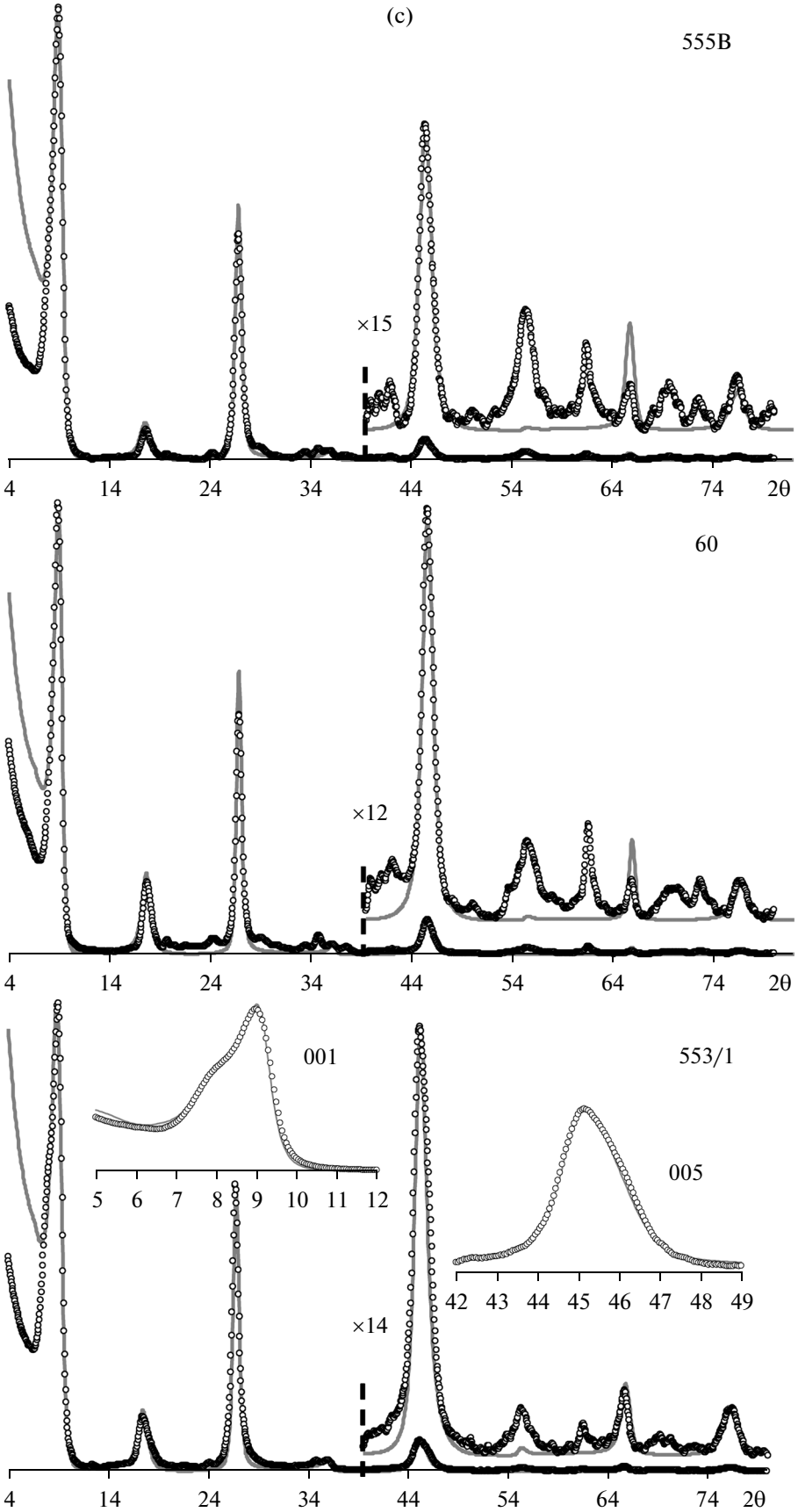
(c)
555B
×15
4 14 24 34 44 54 64 74 2θ
60
×12
4 14 24 34 44 54 64 74 2θ
001
5 6 7 8 9 10 11 12
553/1
005
42 43 44 45 46 47 48 49
×14
4 14 24 34 44 54 64 74 2θ

Fig. 14. Contd.

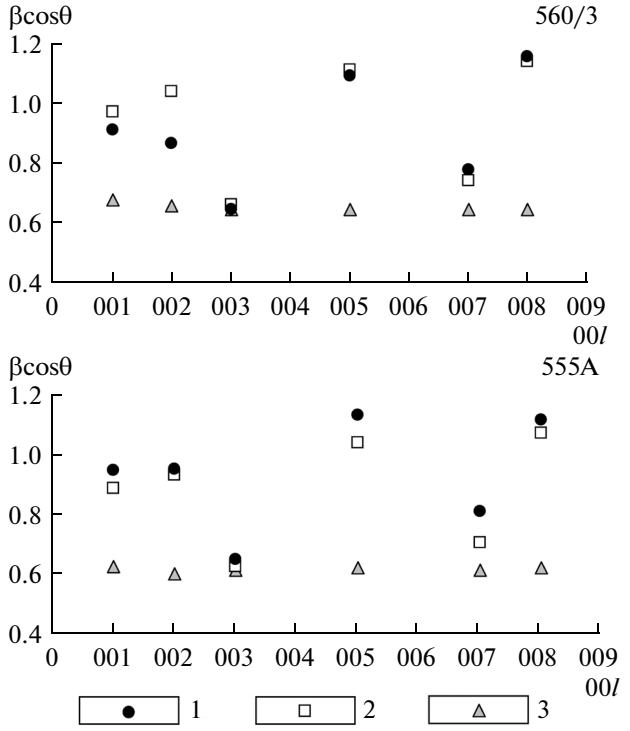

Fig. 15. Comparison of half-widths of basal reflections for samples 555A and 560/3. (1) Experimental; (2) calculated for the mixed-layer structures; (3) calculated for the defect-free structure consisting of micaceous layers, average CSD thickness of which equals to that of the mixed-layer structure.

and the composition of individual 2 : 1 layers that make up micro- and nanocrystals. As shown in (Drits et al., 2010), different degrees of the Si substitution for Al in tetrahedral sheets of micaceous interlayers are responsible for their different thicknesses, which lead to variations in the interlayer, and, consequently, layer (2 : 1 layer + interlayer) thicknesses. In natural mixed-layer structures dominated by micaceous interlayers, their thickness also could vary, relative to their average thickness, owing to the heterogeneous cationic composition of 2 : 1 layers. In a general case, variations of layer thicknesses are described by the function of statistical distribution of true distances corresponding to true thicknesses of micaceous layers. Depending on the nature of interaction between layers, variations of the first and second order are recognized (Guinier, 1964; Drits and Tchoubar, 1990). Distribution of the first-order variation is similar for any layer pair in the considered layer succession. This denotes that the short- and long-range order of distribution of true layer thicknesses in such succession is defined by the same law. Second-order variations show no long-range order in their distribution. This denotes that variations in thickness of the interlayer space between a certain pair of 2 : 1 layers do not depend on those in the adjacent interlayer separating another pair of 2 : 1 layers. The presence of the first-order defects does not affect the profile of basal reflections, but they are accompanied by the subsequent decrease of their intensity with the growth of the reflection order l. For the second-order variations, growth of the order of basal reflections l is associated with decrease of the intensity and broadening of these reflections. Simulation of intensities and shapes of basal reflections of natural mixed-layer structures is based on mathematical formalism, in which second-order variations in the layer thickness are controlled by the normal Gaussian distribution having a standard deviation $\Delta\xi$ (Drits and Tchoubar, 1990).

Taking into account all these facts, the systematic broadening of experimental basal reflections with $l \geq 5$, relative to the calculated ones, may be attributed to second-order variations in thicknesses of the micaceous interlayers. Calculations of diffraction patterns, which took into account the above mentioned structural parameters and variations in the thickness of micaceous layers with standard deviation $\Delta\xi = 0.06$ Å, showed very close $(\beta\cos\theta)_e$ and $(\beta\cos\theta)_c$ values corresponding to reflections 005, 007, and 008. This effect is well seen from the comparison of Q dependence on $(\beta\cos\theta)_e$ and $(\beta\cos\theta)_c$ calculated for mixed layer structures with $\Delta\xi = 0$ and the same structures with the thickness of mica layers varying with standard deviation $\Delta\xi = 0.06$ Å (samples 400/3, 555B; Figs. 13b, 13c).

At the same time, close values of $(\beta\cos\theta)_e$ and $(\beta\cos\theta)_c$ are observed in sample 560/3 for all reflections regardless of their indices, except for reflection 002. This presumably indicates the minimum probability of second-order variations of layer thickness in structure of this sample. More significant and nonsystematic differences between comparable $(\beta\cos\theta)_e$ and $(\beta\cos\theta)_c$ values observed in other samples are possibly related to the measurement error in the half-widths of experimental reflections and the calculation of averaged CSD thickness based on the assumption that the half-width of reflection 003 does not depend on the content of smectite layers.

True Structure of Sample 553/1

Distribution of experimental $(\beta\cos\theta)_e$ and calculated $(\beta\cos\theta)_c$ half-widths with Q values in sample 553/1 differs from that in all other studied samples, on the one hand, in the highest content of smectite layers (12.6%) determined from the slope of experimental regression straight line, and on the other hand, in significant difference between slope angles of experimental ($\alpha_e = 24.0°$) and calculated ($\alpha_s = 29.6°$) regression straight lines and as result, in different W_{Sm} equal 12.6% and 10.3%, respectively (Fig. 13c). In order to explain such unusual distribution of $(\beta\cos\theta)_e$ and $(\beta\cos\theta)_c$, let us consider two significant features of the experimental XRD pattern (Fig. 14c). First, it is well seen in the figure that the calculated profile of reflec-

tion 005 is much narrower than the experimental one. Second, the careful consideration of experimental and calculated profiles of reflection 001 showed that the calculated profile in its upper half is wider than the experimental one and vice versa. This feature allowed us to suggest that the distribution of smectite and micaceous layers is not completely random, but is controlled by the short-range order factor $R \geq 1$. Simulation of the experimental pattern performed by the trial-and-error method for different structural models showed that the best fit between experimental and calculated diffraction patterns was attained for the model, in which the 9.99 Å micaceous layers are alternated with 13.2 and 16.75 Å smectite layers at $R = 2$. Let us designate the micaceous, 16.75 and 13.2 Å smectite layers by letters *A, B*, and *C*, respectively. As already mentioned, the alternation of different layers with maximum possible degree of order at $R = 2$ denotes that the probability of occurrence of two adjacent smectite layers equals zero ($P_{BB} = P_{CC} = 0$), and smectite layer in the structure must be separated by at least two micaceous layers. The latter implies that the probability to discover triplets, such as *BAB, BAC, CAB*, and *CAC*, should be zero. The condition that $P_{BB} = P_{CC} = P_{CB} = P_{BC} = 0$ predetermines the zero probability to meet triple smectite layers *BBB, BBC, BCC, CBC, CCC, CCB, CBB,* and *BCB*. At all known zero probability parameters and contents of layers of different types ($W_A = 0.87$, $W_B = 0.10$, $W_C = 0.03$), the non-zero probability parameters, such as P_{AA}, P_{AAA}, P_{ABA} and so on, were calculated from equations relating all zero and non-zero probability coefficients required to describe three-component mixed-layer systems, in which layers of different types are alternated with maximum possible degree of order at $R = 2$. Detailed description of such equations and calculation of parameters for the given type of structure are given in (Sakharov and Lanson, 2013). Fragments demonstrating the degree of correspondence between the experimental and calculated profiles of reflections 001 and 005 are shown in the inset in Fig. 14c (sample 553/1). It is worth to mention that the total content of smectite layers in the three-component structure seemed to be 13%. This value within error coincides with $W_{Sm} = 12.6\%$, which was determined from the slope angle of the experimental regression straight line. At the same time, the content of smectite layers (10.3%) determined from the slope angle of regression straight line calculated for the two-component structure at $R = 0$ was equal to the content of 16.75 Å layers in the three component structure.

CONCLUSIONS

On the basis of detailed analysis and simulation of diffraction effects from mixed-layer structures, we have developed a technique for determining the low contents of smectite layers in the finely dispersed K-bearing micaceous minerals. Systematic analysis was carried out for diffraction patterns recorded from structures, in which the prevailing 9.98 Å micaceous layers are alternated with 16.85 Å smectite layers in different proportions and at different shortrange order factors ($R \geq 0$). The obtained data made it possible to propose a simple procedure based on the calculation of full width at the half-thickness of basal reflections for the determination of the content of alternating layers in the two-component mixed-layer structure, the average thickness, and the average number of layers in the averaged CSD. Efficiency of this technique was testified on the monomineral dispersed K-bearing micaceous varieties of illite–glauconite composition. It was shown that the content of smectite layers in the studied samples varies from 5.2 to 12.6%. For each of the studied samples, we calculated diffraction patterns of structural models, with the structural parameters (content and composition of alternating layers, thickness and number of layers in the averaged CSD) obtained from the analysis of experimental data. The contents of smectite layers determined by the measurement of half-width of basal reflections in the calculated XRD patterns coincided within 0.2–0.5% with their experimentally determined contents. Moreover, the detailed analysis of half-widths of the experimental and calculated basal reflections with similar *l* values made it possible to distinguish structures, which lack or include the second-order variations in the thicknesses of micaceous layers. The results demonstrated that application of the proposed technique provides a reliable quantitative information on the low content of smectite layers ($W_{Sm} < 10–12\%$) and some specific structural features of the natural dispersed dioctahedral micaceous varieties.

At the same time, theoretical and experimental studies indicate the necessity to expand the potential opportunities of the considered technique by theoretical and experimental works in the following main directions.

First, it is necessary to take into account the effect of different thicknesses of the alternating micaceous and smectite layers. It is known that the thickness of micaceous layers (2 : 1 layer + interlayer) varies from 10.02 to 9.90 Å while passing from high-Al illites to high-Mg aluminoceladonites (Drits et al., 2010). Possible changes in the thickness of the ethylene glycol-saturated smectite layers were noted in (Środoń, 1980). The task was to exclude the influence of the thickness of alternating layers on the half-width of basal reflections during calculation of the content of smectite layers in the studied sample structure.

Second, it is necessary to identify three-component structures, which contain not only micaceous and smectite layers, but also a very small amount of either vermiculite-type layers or ditrioctahedral chlorite layers. The real existence of the three-component mixed-layer structure made up of alternating micaceous, 16.85 Å smectite, and 13.2 Å vermiculite-type layers at $R = 2$ was established in this work and in

papers of other authors (Lanson et al., 2009; Sakharov et al., 1999). This problem may be solved by the diffraction analysis of samples in natural and ethylene glycol-saturated states with the simultaneous study of trends in variations of half-widths of the experimental basal reflections and their spacings.

An important problem is the continuation of works on establishing the short-range order in the alternation of different types of layers, especially during the study of structures containing >10% smectite layers. In solving this problem, attention should be focused not only on the half-width, but also on the symmetry of the analyzed reflection profile.

At last, the structural–crystallochemical features of micaceous mineral varieties responsible for the extremely narrow profile of reflections 002 have yet to be determined.

ACKNOWLEDGMENTS

This work was supported by the Russian Foundation for Basic Research, project no. 12-05-00381.

REFERENCES

Drits, V.A. and Sakharov, B.A., *Rentgenostrukturnyi analiz smeshanosloinykh mineralov* (The X-Ray Structural Analysis of Mixed-Layer Minerals), Moscow: Nauka, 1976.

Drits, V.A. and Tchoubar, C., *X-ray diffraction by disordered lamellar structures*, New York: Springer, 1990.

Drits, V.A. and Kossovskaya, A.G., *Glinistye mineraly: smektity, smeshanosloinye obrazovaniya* (Clay Minerals: Smectites and Mixed-Layer Varieties), Moscow: Nauka, 1990.

Drits, V.A. and Kossovskaya, A.G., *Glinistye mineraly: slyudy, khlority* (Clay Minerals: Micas and Chlorites), Moscow: Nauka, 1991.

Drits, V.A., Kameneva, M.Yu., Sakharov, B.A., et al., *Problemy opredeleniya real'noi struktury glaukonitov i rodstvennykh tonkodispersnykh fillosilikatov* (Problems of Determination of the Real Structure of Glauconites and Related Fine-Dispersed Phyllosilicates), Novosibirsk: Nauka, 1993.

Drits, V.A., Varaxina, T.V., Sakharov, B.A., and Plançon, A., A simple technique for identification of one-dimensional powder X-ray diffraction patterns for mixed-layer illite-smectites and other interstratified minerals, *Clays Clay Miner.*, 1994, vol. 42, pp. 382–390.

Drits, V.A., Środoń, J., and Eberl, D.D., XRD measurements of mean crystallite thickness of illite and illite/smectite: Reappraisal of the Kubler index and the Scherrer equation, *Clays Clay Miner.*, 1997a, vol. 45, pp. 461–475.

Drits, V.A., Sakharov, B.A., Lindgreen, H., and Salyn, A., Sequential structural transformation of illite-smectite-vermiculite during diagenesis of Upper Jurassic shales from North Sea and Denmark, *Clay Miner.*, 1997b, vol. 32, pp. 351–371.

Drits, V.A., Sakharov, B.A., Dainyak, L.G., et al., Structural and chemical heterogeneity of illite-smectites from Upper Jurassic mudstones of East Greenland related to volcanic and weathered parent rocks, *Am. Miner.*, 2002a, vol. 87, no. 12, pp. 1590–1607.

Drits, V.A., Lindgreen, H., Sakharov, B.A., et al., Tobelitization of smectite during oil generation in oil-source shales. Application to North Sea illite-tobelite-smectite-vermiculite, *Clays Clay Miner.*, 2002b, vol. 50, pp. 82–98.

Drits, V.A., Sakharov, B.A., A.L. Salyn, and H. Lindgreen, Determination of the content and distribution of fixed ammonium in illite-smectite using a modified X-ray diffraction technique: Application to oil source rocks of western Greenland, *Am. Miner.*, 2005, vol. 90, pp. 71–84.

Drits, V.A., Zviagina, B.B., McCarty, D.K., and Salyn, A.L., Factors responsible for crystal-chemical variations in the solid solutions from illite to aluminoceladonite and from glauconite to celadonite, *Am. Miner.*, 2010, vol. 95, pp. 348–361.

Drits, V.A., Ivanovskaya, T.A., Sakharov, B.A., et al., Nature of the Structural and Crystal-Chemical Heterogeneity of the Mg-Rich Glauconite (Riphean, Anabar Uplift), *Lithol. Miner. Resour.*, 2010, no. 6, pp. 555–567.

Drits, V.A, Ivanovskaya, T.A., Sakharov, B.A., et al., Mixed-Layer Corrensite–Chlorites and Their Formation Mechanism in the Glauconitic Sandstone–Clayey Rocks (Riphean, Anabar Uplift), *Lithol. Miner. Resour.*, 2011, no. 6, pp. 566–593.

Guinier, A., *Theorie et technique de la radiocristallographie*, Paris: Dunod, 1964.

Ivanovskaya, T.A., Zaitseva, T.S., Zvyagina, B.B., and Sakharov, B.A., Crystal-Chemical Peculiarities of Globular Layer Silicates of the Glauconite–Illite Composition (Upper Proterozoic, Northern Siberia), *Lithol. Miner. Resour.*, 2012, no. 6, pp. 499–520.

Lanson, B., Sakharov, B.A., Claret, F., and Drits, V.A., Diagenetic smectite-to-illite transition in clay-rich sediments: a reappraisal of X-ray diffraction results using the multi-specimen method, *Am. J. Sci.*, 2009, vol. 309, no. 6, pp. 476–516.

Lindgreen, H., Drits, V.A., Sakharov, B.A., et al., The structure and diagenetic transformation of illite-smectite and chlorite-smectite from North Sea Cretaceous-Tertiary chalk, *Clay Miner.*, 2002, vol. 37, pp. 429–450.

Lindgreen, H., Drits, V.A., Jakobsen, F.C., and Sakharov, B.A., Clay mineralogy of the Central North Sea Upper Cretaceous-Tertiary chalk and formation of clay rich layers, *Clays Clay Miner.*, 2008, vol. 56, pp. 693–710.

McCarty, D.K., Sakharov, B.A., and Drits, V.A., Early clay diagenesis in Gulf Coast sediments: new insights from XRD profile modeling, *Clays Clay Miner.*, 2008, vol. 56, no. 3, pp. 359–379.

McCarty, D.K., Sakharov, B.A., and Drits, V.A., New insights into smectite illitization: A zoned K-bentonite revisited, *Am. Miner.*, 2009, vol. 94, pp. 1653–1671.

Mering, J., L'interference des Rayons X dans les systems a stratification desordonnee, *Acta Crystallogr.*, 1949, vol. 2, pp. 371–377.

Moore, D.M. and Reynolds, R.C., Jr., *X-Ray Diffraction and the Identification and Analysis of Clay Minerals*, Oxford: Oxford Univ. Press, 1989.

Moore, D.M. and Reynolds, R.C., Jr., *X-Ray Diffraction and the Identification and Analysis of Clay Minerals*, Oxford: Oxford Univ. Press, 1997.

Reynolds, R.C., Jr., and Hower, J., The nature of interlayering in mixed-layer illite-montmorillonites, *Clays Clay Miner.*, 1970, vol. 18, pp. 25–36.

Reynolds, R.C., Interstratified clay minerals, in *Crystal Structures of the Clay Minerals and Their X-Ray Identification*, Brindley, G.W. and Brown, G., Eds., London: Miner. Soc., 1980, pp. 249–303.

Reynolds, R.C., *NEWMOD, a Computer Program for the Calculation of One-Dimensional Diffraction Patterns for Mixed-Layered Clays*, Reynolds, R.C., Ed., Hanover: New Hampshire, 1985.

Reynolds, R.C., The Lorentz-polarization factor and preferred orientation in oriented clay aggregates, *Clays Clay Miner.,* 1986, vol. 34, pp. 359–367.

Reynolds, R.C., Mixed-layer chlorite minerals, in *Hydrous Phyllosilicates. Reviews in Mineralogy*, Washington, DC: Miner. Soc. Am., 1988, vol. 19, pp. 601–609.

Sakharov, B.A., Besson, G., Drits, V.A., Kameneva, M.Yu., Salyn, A.L., and Smoliar, B.B., X-ray study of the nature of stacking faults in the structure of glauconites, *Clays Clay Miner.*, 1990, vol. 25, pp. 419–435.

Sakharov, B.A. and Lanson, B., X-ray identification of mixed-layer structures, in *Handbook of Clay Science, Part B. Techniques and Applications*, Bergaya, F. and Lagaly, G., Eds., Amsterdam: Elsevier, 2013, Chapter 2.3 (Modeling of Diffraction Effects), pp. 51–135.

Sakharov, B.A., Lindgreen, H., Salyn, A.L., and Drits, V.A., Determination of illite-smectite structures using multispecimen X-ray diffraction profile fitting, *Clays Clay Miner.*, 1999, vol. 47, pp. 555–566.

Środoń, J., Precise identification of illite-smectite interstratification by X-ray powder diffraction, *Clays Clay Miner.*, 1980, vol. 28, pp. 401–411.

Środoń, J., X-ray identification of randomly interstratified illite/smectite in mixtures with discrete illite, *Clay Miner.*, 1981, vol. 16, pp. 297–304.

Środoń, J., X-ray powder diffraction identification of illitic materials, *Clays Clay Miner.*, 1984, vol. 32, pp. 337–349.

Środoń, J., Use of clay minerals in reconstructing geological processes: recent advances and some perspectives, *Clay Miner.*, 1999, vol. 47, pp. 27–37.

Środoń, J. and Eberl, D., Illite, in *Micas. Reviews in Mineralogy*, Washington, DC: Miner. Soc. Am., 1984, vol. 13, pp. 495–544.

Środoń, J., Morgan, D.J., Eslinger, E.V., et al., Chemistry of illite/smectite and end-member illite, *Clays Clay Miner.*, 1986, vol. 34, pp. 368–378.

Watanabe, T., Identification of illite/montmorillonite interstratifications by X-ray powder diffraction, *J. Miner. Soc. Jap. Spec. Iss.,* 1981, vol. 15, no. pp. 32–41.

Wojdyr, M., Fityk: a general-purpose peak fitting program, *J. Appl. Crystallogr.*, 2010, vol. 43, pp. 1126–1128.

Translated by M. Bogina